Durham University

Durham Research Online

Deposited in DRO:

11 February 2015

Version of attached file:

Accepted Version

Peer-review status of attached file:

Peer-reviewed

Citation for published item:

Brown, R.J. and Manya, S. and Buisman, I. and Fontana, G. and Field, M. and Niocaill, C.M. and Sparks, R.S.J. and Stuart, F.M. (2012) 'Eruption of kimberlite magmas: physical volcanology, geomorphology and age of the youngest kimberlitic volcanoes known on earth (the Upper Pleistocene/ Holocene Igwisi Hills volcanoes, Tanzania).', Bulletin of volcanology., 74 (7). pp. 1621-1643.

Further information on publisher's website:

http://dx.doi.org/10.1007/s00445-012-0619-8

Publisher's copyright statement:

The final publication is available at Springer via http://dx.doi.org/10.1007/s00445-012-0619-8

Additional information:

Use policy

The full-text may be used and/or reproduced, and given to third parties in any format or medium, without prior permission or charge, for personal research or study, educational, or not-for-profit purposes provided that:

- a full bibliographic reference is made to the original source
- a link is made to the metadata record in DRO
- the full-text is not changed in any way

The full-text must not be sold in any format or medium without the formal permission of the copyright holders.

Please consult the full DRO policy for further details.

Durham University Library, Stockton Road, Durham DH1 3LY, United Kingdom
Tel : +44 (0)191 334 3042 | Fax : +44 (0)191 334 2971
http://dro.dur.ac.uk

Eruption of Kimberlite Magmas: Physical volcanology, Geomorphology, and Age of the Youngest Kimberlitic Volcanoes known on Earth (the Upper Pleistocene/Holocene Igwisi Hills volcanoes, Tanzania)

Richard J. Brown[1*], S. Manya[2], I. Buisman[3], G. Fontana[4], M. Field[5], C. Mac Niocaill[4], R.S.J. Sparks[6], F.M. Stuart[7]

[1]Department of Earth and Environmental Sciences, Open University, Walton Hall, Milton Keynes MK7 6AA, UK
[2]Department of Geology, University of Dar es Salaam, Dar es Salaam, Tanzania
[3]Department of Earth Sciences, University of Cambridge, Downing Street, Cambridge, CB2 3EQ, UK
[4]Department of Earth Sciences, University of Oxford, Parks Road, Oxford OX1 3PR, UK
[5]AMEC plc, Environment & Infrastructure - Growth Regions (Mining Services Group) International House, Dover Place, Ashford, TN23 1HU
[6]Department of Earth Sciences, Wills Memorial Building, University of Bristol, Queen's Road, Bristol BS7 1RJ, UK
[7]Isotope Geosciences Unit, SUERC, Scottish Enterprise Technology Park, East Kilbride, G75 0QF, UK
*Now at: Department of Earth Sciences, Durham University, Science Labs, Durham, DH1 3LE, UK
Contact: richard.brown3@durham.ac.uk

Abstract

The Igwisi Hills volcanoes (IHV), Tanzania, are unique and important in preserving extra-crater lavas and pyroclastic edifices. They provide critical insights into the eruptive behaviour of kimberlite magmas that are not available at other known kimberlite volcanoes. Cosmogenic ^{3}He dating of olivine crystals from IHV lavas and palaeomagnetic analyses indicates that they are Upper Pleistocene to Holocene in age. This makes them the youngest known kimberlite bodies on Earth by >30 Myr and may indicate a new phase of kimberlite volcanism on the Tanzania craton. Geological mapping, GPS surveying and field investigations reveal that each volcano comprises partially eroded pyroclastic edifices, craters and lavas. The volcanoes stand <40 m above the surrounding ground and are comparable in size to small monogenetic basaltic volcanoes. Pyroclastic cones consist of diffusely layered pyroclastic fall deposits comprising scoriaceous, pelletal and dense juvenile pyroclasts. Pyroclasts are similar to those documented in many ancient kimberlite pipes, indicating overlap in magma fragmentation dynamics between the Igwisi eruptions and other kimberlite eruptions. Characteristics of the pyroclastic cone deposits, including an absence of ballistic clasts and dominantly poorly vesicular scoria lapillistones and lapilli tuffs indicate relatively weak explosive activity. Lava flow features indicate unexpectedly high viscosities (estimated at $>10^2$ to 10^6 Pa s) for kimberlite, attributed to degassing and in-vent cooling. Each volcano is inferred to be the result of a small-volume, short-lived (days to weeks) monogenetic eruption. The eruptive processes of each Igwisi volcano were broadly similar and developed through three phases: (1) fallout of lithic-bearing pyroclastic rocks during explosive excavation of craters and conduits (2) fallout of juvenile lapilli from unsteady eruption columns and the construction of pyroclastic edifices around the vent; and (3) effusion of degassed viscous magma as lava flows. These processes are similar to those observed for other small-volume monogenetic eruptions (e.g., of basaltic magma).

Keywords: kimberlite; Igwisi Hills; explosive eruption; lava; monogenetic volcano

Introduction

Eruptions of ultrabasic kimberlite magmas have never been witnessed, and the dynamics of the magma's ascent, degassing or dispersal as pyroclasts and lavas at the surface are not well understood. They are characterised by very low silica contents, high volatile contents and inferred low magmatic viscosities (Mitchell 1986; Sparks et al. 2006). They originate from great depths (>100 km) and entrain host rock from the mantle during ascent. There are over 5000 known kimberlite occurrences dating back to the Early Proterozoic (Kjarsgaard 2007). Due to their great age (>30 Ma) most kimberlites have had their surface rocks removed by erosion. All that remains for study in most cases are the volcaniclastic rocks and intrusions preserved within their subterranean volcanic vents (kimberlite pipes). These rocks are prone to alteration, and primary deposit characteristics are commonly obscured (e.g., Sparks et al. 2006; Cas et al. 2008; Stripp et al. 2008; Buse et al. 2010). Volcaniclastic rocks preserved within kimberlite vents have proved problematic to interpret and a number of different, but not mutually exclusive, processes have been proposed and elaborated for various pipes. These include fluidisation (Dawson 1971; Field and Scott Smith 1999; Sparks et al 2006; Walters et al. 2006; Gernon et al. 2008a and b), phreatomagmatism (Lorenz 1975; Ross and White 2006; Lorenz and Kurszlaukis 2007; Kurszlaukis and Lorenz 2008), eruption column collapse (Porritt et al. 2008) and re-sedimentation (Moss et al. 2008).

The Igwisi Hills kimberlite volcanoes (IHV; Sampson 1953; Reid et al. 1975; Dawson 1994) are thought to be very young (Quaternary) but no reliable radiometric dates have yet been published. The next youngest kimberlite rocks are Eocene-Oligocene in age (the Kundelungu plateau pipes, Democratic Republic of Congo, Batumike et al. 2009). Because of their youth, the IHV still preserve surface rocks and volcanic constructs at the Earth's surface. Kimberlite volcanic rocks emplaced on the Earth's surface, as opposed to within vents, have great potential to provide insight into eruptive dynamics, much as they have for other volcanic systems. Examples include bedded and stratified pyroclastic rocks within ancient kimberlite craters (e.g., Mwadui, Tanzania, Stiefenhofer and Farrow2004; Orapa A/K1, Botswana, Field et al. 1997,Gernon et al. 2009a and b, Fontana et al., 2011; Jwaneng, Botswana, Brown et al. 2008b; Victor pipe, Canada, van Straaten et al., 2011). Extra-crater examples are rare with the best known being the Fort a la Corne kimberlites, Canada, which have been intersected by numerous drill cores and interpreted as volcanoes preserving extra-crater rocks (Berryman et al. 2004; Zonneveld et al. 2004, Kjarsgaard et al. 2007; Pittari et al. 2006). Another example is the Tokapal kimberlite, India (Mainkar et al. 2004).

We present a new geological map for the IHV, and describe and interpret the volcanoes' morphology, field relationships, lithofacies, macro-scale features and petrography. We present new geochronological data that confirms a very young (almost Holocene) age for the IHV. We then compare the IHV to other monogenetic volcanoes and with kimberlite pipes.

Geological Setting and previous work

The IHV are located on the western side of the Archaean Tanzanian craton, 27kilometres NW of the village of Urambo (Fig.1). They were emplaced through granitic gneiss basement of the 2500 ±100 Ma Dodoman system (see Bell and Dodson 1981). The basement outcrops in small rounded kopjes near Igwisi village and there are xenoliths in the lavas and pyroclastic rocks. The IHV were first recognised by the Tanganyikan Geological Survey in the early 1950s (Sampson 1953; Basset 1954; Fozzard 1956; Dawson 1964). Subsequent studies focused mainly on the petrology of the lava flow from the NE volcano and its mantle xenoliths(Mitchell 1970; Dawson 1971; Reid et al. 1975; Dawson 1994). Reid et al. (1975) and Dawson (1994) considered that the Igwisi melts originated at >110 km depth and concluded that the mineralogy, major element and isotope chemistry of the Igwisi Hills rocks have strong affinities with calcite-rich kimberlites (e.g. Benfontein sills, South Africa, Dawson and Hawthorne 1973; see also Mitchell 2008). Mitchell (2008) considered that the IVH magmas depart from the composition of typical kimberlites due to the presence of hercynitic groundmass spinels that

indicate significant crustal contamination. Our geochemical studies (Willcox et al., submitted) of the IVH support the conclusions of Reid et al. (1975) and Dawson (1994) that they are geochemically similar to calcitic kimberlites. Little has been published about the physical volcanology of the volcanoes, except that they are three volcanic centres comprising cones and craters of pyroclastic rocks and lavas (Sampson 1953; Dawson 1994).

The IHV represent the youngest volcanic activity on the Tanzanian craton, which previously experienced phases of kimberlite volcanism at around 189 Ma (Davis 1977) and 53 Ma (Davis 1977; Haggerty et al. 1983; Gobba 1989). The IHV are considered the youngest kimberlite volcanoes on Earth. Dawson (1994) suggested that they are Quaternary in age based on morphological comparisons with known Quaternary volcanoes in northern Tanzania.

Methodology

Field study

We undertook detailed geological mapping and sampling of the IHV. Real time kinetic surveying of the volcanoes was undertaken using a Leica 1200 differential GPS system. Depending on the terrain, radial, circumferential or orthogonal survey grids with a spacing of <50 m were walked out. Morphological features, such as ridges, scarps and crater walls, and geological boundaries were surveyed separately as breaklines. These data were processed in ARCGIS™ to create a DEM that was then contoured at 2 m intervals (Fig. 2). The DEM was populated with >50 000 xyz points each of which typically had an accuracy of <1 cm. Several shallow trenches were dug to examine the subsurface geology away from the volcanoes. We also report the results of petrographic study of the rocks. Vesicularity, lithic contents and mineral phase abundances were calculated from photographs of hand specimens and thin sections using ImageJ software (http://rsbweb.nih.gov/ij/), and are reported as volume abundances. The volumes of the volcanic rocks were calculated using 3D models constructed in Gemcom GEMS™ 3D modeling software from the xyz survey data. We use standard volcanological and pyroclastic terminology throughout (e.g., Cas and Wright1987; White and Houghton 2006). Semi-quantitative grainsize data and sorting parameters for lithofacies were computed in the lab from 1000 length measurements of particles extracted from suitable photographs.

Cosmogenic ^{3}He dating

Three samples were taken for cosmogenic He exposure dating. One sample (IH15) was taken from the eastern summit of the lava coulée of the central volcano under very sparse woodland (Fig. 2). Two samples (IH52 and IH61) were taken from the NE volcano. Sample IH61 was collected from the weathered upper parts of the lava flow under sparse woodland (Fig. 2 and 3A). Sample IH52 is from a scarp cut through the interior of the lava along the eastern crater wall (Fig. 2 and 3B). Samples IH15 and IH61 were considered to be close to the original surface of the lava flows (<1 m). Sample IH52 represents an exposed footwall generated during late-stage subsidence in the NE crater.

Olivine was concentrated from the 0.5–1 mm fraction of crushed samples using magnetic and density techniques. Concentrates were ultrasonically cleaned in 20% HNO_3 and distilled water, and a pure separate was picked under a binocular microscope. Altered grains and those with adhering basalt or iron oxide tarnish were removed and the pure separate cleaned in deionized water and then analar acetone. Magmatic He in trapped gas inclusions was extracted from approximately 1 g of olivine by crushing in vacuum in an all-metal multi-sample hydraulic crusher. The lattice-hosted He was extracted from approximately 250 mg of the 100–200 μm grain olivine that remained after crushing. Each sample was melted during a 20-minute heating period using an 808 nm diode laser (Foeken et al. 2007). In the case of IH52, two splits were analysed (Table 1). Re-heating after initial melt step yielded no significant cosmogenic He. Gas clean up procedures and mass spectrometric techniques for helium isotope ratio determination are reported by Williams et al. (2005). Blank levels for both extraction

techniques are governed by the helium background in the mass spectrometer and average 5 x $10^3$and 5 x 10^8atoms of ^{3}He and ^{4}He respectively. These amounts represent less than 0.1% of the sample helium. The reproducibility of standard He abundance determinations over the two periods of analyses were 1% for ^{3}He and 0.5% for ^{4}He.Analytical uncertainties reported in Table 1 are propagated from uncertainties in the ^{3}He and ^{4}He concentrations.

Palaeomagnetic study

To further help constrain the age of the Igwisi Hills lavas, twenty oriented 25mm diameter cores were collected, using a portable rock drill, from the lava flows for palaeomagnetic analysis. Samples were oriented in the field with sun and magnetic compasses, and were subsequently cut in the laboratory into standard cylindrical specimens, with most cores yielding two or more specimens. A total of 29 specimens from 17 samples were subjected to progressive thermal (14 specimens) or alternating field (AF) (15 specimens) demagnetisation, using a minimum of 14 steps, up to peak temperature of 580°C or peak AF fields of 100mT. The natural remanent magnetisation (NRM) of the specimens was measured at each step with a Molspin Spinner magnetometer or a 2G cryogenic magnetometer housed in a magnetically shielded room at the University of Oxford. Components of magnetisation were identified using principal component analysis of linear segments in the demagnetisation trajectories, where lines were defined by a minimum of five consecutive points.

The Igwisi Hills volcanoes (IHV)

The IHV are three small volcanic centres (NE, central and SW volcanoes) comprising pyroclastic cones, craters and lavas (Fig. 2 and 3C–E). Together they constitute >3.2 × 10^6 m^3 (Table 2) of erupted products and cover >2.7 × 10^5 m^2. The relative ages of the IHV cannot be fully constrained, although field relationships indicate that the central volcano postdates the NE volcano. They are aligned NE–SW and sit upon a broad, low NE–SW-oriented ridge, 500 m wide and 16 m high that is probably composed of pyroclastic material (poorly exposed) from early stages of the eruptions. The volcanoes have been partially buried by younger sediments and soils, and are presently covered in grassland and low-density forest. They exhibit similar pyroclastic lithofacies, which are summarized in Table 3. Pyroclastic rocks are lithified with calcite cement, which means that standard granulometric analyses commonly applied to loose pyroclastic deposits cannot be used. Morphological, structural and lithological features of each volcano are outlined below. Note that many of the large olivine crystals in the IHV are multigrain aggregates and can be regarded as micro mantle xenoliths (Dawson 1994).

NE volcano

The NE volcano covers >1.9 × 10^5 m^2 and comprises a flat-bottomed sub-circular crater ~200 × 200 m in diameter surrounded by a partial low ring of outward-dipping pyroclastic rocks and by lava (Fig. 2 and 3C). The crater floor (1088 masl) is at or just below the inferred height of the palaeo-surface. Crater walls on the northern side of the crater comprise a succession of bedded pyroclastic rocks; the eastern side comprises lava. The northern and western crater walls are presently 4–8 m higher than the eastern crater wall (Fig 2 and 3C).The south-western crater wall has been buried by lava from the central volcano (Fig. 2).

Pyroclastic rocks

The oldest exposed pyroclastic rocks are grey, bedded lithic-bearing coarse tuffs and lapillistones (blT/blL, see Table 3 and Fig. 4). They are exposed along the inner crater wall on the north of the volcano and in patchy outcrops on the ground on the northern exterior of the volcano. Similar tuffs were encountered in a shallow trench dug radially away from the central volcano (trench 1, Fig. 2). They were not encountered in the other trenches dug to depths of >2 m (Fig. 2). These tuffs reach 8 m

thick in the crater wall and we infer that they form a wide apron extending at least several hundred metres away from the NE and central volcanoes, although their base, and the pre-eruption substrate is not exposed and the apron is mostly covered by soil. Along the inner crater wall the abundance of lithic clasts in these pyroclastic rocks varies between 5–40 vol. % with a typical abundance of 5–12 vol. %.There are two types of pyroclasts in this lithofacies. The first are non-vesicular, crystalline and have irregular and amoeboid to subspherical shapes and are up to several millimetres in diameter (Fig. 5A). The second (pelletal clasts) comprise lithic clasts, olivine crystals and olivine micro-xenoliths surrounded by a thin, uneven coating of solidified kimberlite magma (Fig. 5A).

Overlying the lithic-bearing lithofacies on the north and north-east side of the NE volcano are juvenile clast-rich pyroclastic deposits. These comprise bedded juvenile-rich tuffs and lapillistones (bT/bL), and pelletal clast-rich tuffs and lapillistones (bpelT/bpelL, Table 3;e.g., Fig. 6). Together they exceed 10 m in thickness and are inferred to have originally formed a partial cone with a preserved volume of 3.1×10^5 m^3. No pattern was recognised in the alternation of the two lithofacies. Individual beds are typically 3–30 cm thick and are not traceable between outcrops (i.e. over metres to 10s-of-metre scale) due to an absence of marker horizons and poor outcrop quality. Bedding is defined by changes in grainsize or by alternations between the two lithofacies. Normal-graded, reverse-graded and non-graded beds are present. Beds dip outwards from the crater at angles of 16–28° with an average dip of 21° (Fig. 2). In the south-east of the volcano ~4 m of poorly exposed tuff and lapillistone outcrop between the NE volcano lava and the central volcano (Fig. 2).Similar rocks are poorly exposed beneath lavas in the NE crater wall (Fig. 2).

Three types of pyroclasts occur within these juvenile-rich pyroclastic deposits. The first type is incipiently vesicular scoria clasts up to coarse lapilli size with irregular, angular shapes (e.g., Fig. 5B and C). The edges of the scoria clasts cut through vesicles and there is no evidence for vesicle zoning or chilled exteriors. These have 10–20 vol. % subspherical, elongate to irregular-shaped vesicles, 0.02–3 mm in diameter, some of which show evidence for coalescence (Fig. 5C). Vesicles have been partially filled with secondary calcite. The second are pelletal lapilli comprising olivine crystals and micro-xenoliths which reach 10 mm in diameter. They are coated in a thin jacket of crystalline kimberlite groundmass, which is typically a few 10s of μm thick (Fig. 5D), but in many cases only partially encloses the central grain. The third type are olivine aphyric sub-spherical, rounded dense juvenile lapilli <3 cm in diameter. These latter pyroclasts are rare, accounting for <2–5 % of the pyroclast populations.

Lava

The eastern sector of the NE volcano comprises predominantly kimberlite lava (Fig. 2 and 3C). The mineralogy and petrology of the lava have been described and discussed in detail by both Reid et al (1975) and Dawson (1994), and here we concentrate on physical features. The lava's original upper surface is not preserved, but it overlies poorly exposed lithic-rich tuffs and is at least 2.6 m thick. It is generally poorly exposed along the eastern inner crater wall, and is mostly buried under soil and younger sediments away from the volcano (Fig. 2). The best section through the lava is in the NE sector of the volcano to the east of a prominent notch in the crater walls (Fig. 2). It has a fine-grained crystal-poor base and an olivine crystal- and micro-xenolith-rich lower third (Fig. 7). Imbricated olivine crystals and xenoliths within the lava indicate flow towards the SSW, i.e. back into the crater. Large olivine crystals and micro-xenoliths vary in abundance through the lava, but generally decrease in abundance upwards (from 26 vol. % to 5 vol. %), above the thin olivine-poor base (Fig. 6). The upper parts of the lava are poorly vesicular (<15 vol. %). Vesicles vary from 1–40 mm in diameter, are sub-spherical to irregular in shape and some are sheared and coalesced (Fig. 7). Most vesicles are lined with a thin coating of carbonate.

The lava forms a broad irregular eroded plateau-like feature, ~200 m long by 100 m wide, on the eastern side of the volcano and exhibits metre-scale topography (Fig. 2 and 3C). The plateau rises up to 16 m above the crater floor (Fig. 2) and exhibits a crudely-defined, stepped morphology down into the crater over a distance of<50 m. The plateau passes into a flat-lying poorly exposed lava flow that extends northeast for >500 m. The lobate margin of the latter lava flow (Fig. 2) has been defined by scattered outcrops and by the location of loose lava blocks and boulders on the forest floor. The lava forming the eastern plateau overlies a thin wedge of outward-dipping pyroclastic rocks exposed beneath the lava in the NE and SE crater wall (Fig. 2).In total, lava from the NE volcano covers >1.5 × 10^5 km^2 (including lava in the crater) and assuming an average thickness of 2.5 m it has a minimum volume of >3.7 × 10^5 m^3. The flat-lying lava flow covers 8 × 10^4 m^2 and, assuming a similar average thickness, has a volume of ~2 × 10^5 m^3. Lava is not exposed on the northern or western walls of the crater, but is inferred to underlie the gently inward-dipping margins of the crater along the north and west sides of the crater (Fig. 2).

Central volcano

Morphology and physical structure

The central volcano covers >8.1 × 10^4 m^2 and has a minimum basal diameter of >300 m. It is surrounded to the west and north-west by an eroded apron of lithic-bearing coarse tuff (Fig. 2). The western side comprises a N–S oriented elongate partial cone of outward-dipping bedded pyroclastic rocks, in which beds dip towards the W, NW and SW (Fig. 2 and 3D). This pyroclastic mound rises 36 m above the surrounding plain and has outer slopes of ~24°. The eastern margin of the mound is an N–S oriented, near-vertical crater wall. The crater currently sits beneath a thick lava flow (Fig. 2 and 3D).

Pyroclastic rocks

The pyroclastic cone has a minimum volume of 1.4 × 10^5 m^3 and comprises bedded juvenile-rich lapillistone, lapilli-tuffs and tuffs (bT/bL and bpelT/bpelL, Fig. 6A-F, Table 3) that are texturally similar to those of the NE volcano. Juvenile clasts reach 7 cm in diameter but most are <1.5 cm in diameter. Rare lithic clasts never exceed 10 cm in diameter (Fig. 6F). Tracing individual beds laterally is difficult due to discontinuous outcrops. Thin coarse tuff beds are intercalated with the coarse-grained lapilli-tuff and lapillistone beds and reach several centimetres in thickness. Clasts in these beds have been cemented together with calcite that is absent in the outer 2–3 cm thick weathered rind of most outcrops. Pyroclasts are similar to those found in the pyroclastic deposits of the NE volcano and are described above and in Table 2.Beds in the pyroclastic cone dip outwards at 15–32° (Fig. 2) with an average dip of 21°.

Lava

The crater of the central volcano is filled with a lava flow, which was previously mapped as pyroclastic rocks (see Sampson 1953). It is 150 × 300 m in diameter, is >25 m thick and covers a minimum area of >3.4 × 10^4 m^2 (Fig. 2 and 3D). It has a minimum volume of 4 × 10^5 m^3 (calculated above inferred palaeo-surface). The overall morphology is of a asymmetric mound with two bounding levees either side of a slightly lower central channel open to the southeast. Its western margin abuts against the crater wall of the pyroclastic cone (Fig. 2 and 3D). The northern and eastern slopes of the lava are steep (29–32°) and are partially covered by soil and talus rocks, while the south-west slope is much shallower (2–3°). Its southwest margin is inferred from the position of large blocks of lava and scattered outcrops on the forest floor that define a broad, lobate terminus 180 m wide (Fig. 2).

The lava is dense, homogeneous, reddish-brown, and contains scattered basement inclusions (Fig. 8A and B). Rounded olivine xenocrysts >5 mm account for >2 vol. % of the rock. It has a fine- to medium-grained serpentine-calcite-apatite-spinel-perovskite groundmass. Basement clasts are

commonly recess-weathered and range in diameter from <0.1–8 cm in diameter (Fig. 8A). They are typically rounded and are granitic or dioritic in composition. Unaltered biotite is a prominent constituent of many of the basement inclusions. They are irregularly scattered throughout the lava and reach 2.5–5.5 vol. %. Parallel, curving and cross-cutting centimetre-spaced joint sets are present within the rock.

SW volcano

The SW volcano is located 500 m southwest of the central volcano (centre-to-centre, Fig. 2 and 3E). It comprises a sub-circular pyroclastic cone that covers >8.1 × 10^5 m^2, has a basal diameter of >300 m, and rises over 30 m above the surrounding ground (Fig. 2 and 3E). The north and west walls of the crater are 14 m higher than the south and east side and are breached to the northeast. The slopes of the cone dip ~17° on the west and north and 15° on the east and south (Fig 2). It has a 180 × 140 m flat-bottomed crater perched 12 m above the surrounding ground (Fig. 2).

Pyroclastic rocks

The pyroclastic cone of the SW volcano has a minimum volume of 9 × 10^5 m3.The oldest pyroclastic rocks are massive lithic-bearing tuffs (bT/bL, Table 3), exposed in a 50 m-wide notch on the northern side of the cone (Fig. 3E). They reach several metres thick and also crop out in the surrounding plain up to several 10s metres away from the volcano (Fig. 2). They are compositionally similar to lithic-rich tuffs at the other two volcanoes and look similar in thin-section. They are overlain by 8 metres of massive to bedded juvenile clast-rich lapillistone (mbL, Table 3), which outcrops along the western inner crater wall. This passes upwards into bedded juvenile-rich tuff and lapillistone (bt/bL and bpelT/bpelL, Table 3). Bedding planes dip outwards at 6–31° (Fig. 1) and bedding is steeper on the eastern side of the volcano (<31°) than on the west (<24°; Fig. 2).

Lava

A short, poorly exposed lava crops out at the base of the eastern flank of the SW volcano. Its extent has been estimated by scattered outcrops and by the position of loose lava blocks on the forest floor (Fig. 2). It covers >4000 m^2 and is mostly buried by soil. It is texturally similar to the lava from the NE volcano, is poorly vesicular and contains 5–8 % rounded olivine crystals and olivine micro-xenoliths. Vesicles reach 1 cm in diameter, are highly irregular in shape and account for <12 vol. % of the rock. The base of the lava is not seen and its upper surface is not preserved. It exhibits features similar to shallow levees that run up the eastern side of the pyroclastic cone towards a 30 m wide shallow notch in the crater wall (Fig. 2). It appears to have flowed out of the crater and may indicate that the perched, flat-bottomed crater of the SW volcano is the solidified crust of a lava lake.

Groundmass mineralogy

Petrological aspects and mineral chemistry of the NE lava are described in detail by Reid et al. (1975), Dawson (1994) and Buisman et al. (submitted). Here we outline the key mineralogical features of the Igwisi volcanic products.

Lavas

The dominant mineral phase in the NE lava is olivine, which occurs as spheroidal to ellipsoidal xenocrysts, smaller irregular shaped phenocrysts and as inclusions in titanomagnetite (Fig. 9A, B and C respectively). Olivine crystals exhibit minimal alteration (serpentinisation) and are set in a fine- to medium-grained serpentine-calcite-spinel-apatite-perovskite groundmass (Fig. 10B, C and D). Phlogopite crystals are rare in all samples. Most phlogopite grains are euhedral K-phlogopite with Ba-rich (kinoshitalite) overgrowths (Fig. 9D) with a few either pure kinoshitalite or phlogopite.

Monticellite is present in some samples (Fig. 9E). The spinels are mainly titanomagnetite with thin Mg-Al-spinel rims: a few have Mg-Al-chromite cores (e.g. Fig 9F). Cr-spinel is found as small euhedral inclusions in the olivine xenocrysts.

The NE lava flow exhibits subtle variations: lower parts contain tabular calcite as laths and crystalline grains (Fig. 10D). Some olivine xenocrysts are mantled by perovskite and Mg-Al-spinel at the grain's greatest curvature: this coating thins towards the equator of the grain (Fig. 9A; see Dawson 1994). Groundmass minerals include apatite hopper crystals, perovskite and monticellite. The upper parts of the NE lava show a higher degree of alteration (Fig. 10C). Apatite hopper crystals are filled with serpentine and fine-grained amorphous aggregates of hydrogarnet. Calcite is mostly found as spongy, tabular laths but occasionally as crystalline amorphous aggregates. Most spinels show partial replacement of Mg-Al-spinel rims by hydrogarnet, but some are completely replaced and occur as spinel pseudomorphs consisting of serpentine rims enclosing hydrogarnet (Fig 9G). Serpentine replacing olivine and in the groundmass has an unusual Al-rich composition and has been recognised as a new variety consisting of interlayers of end member serpentine and hydrotalcite (Willcox et al., submitted).

The mineralogy of the central (Fig. 10B) and SW volcanoes' lavas is closely similar to that of the NE lava flow. The rims of olivine xenocrysts are partially resorbed and some smaller forsteritic xenocrysts are pseudomorphed by serpentine, brucite and calcite. The groundmass is mostly serpentine and calcite with small amorphous grains of apatite, hydrogarnet and perovskite. The SW and central volcano lavas exhibit greater abundances of hydrogarnet in the groundmass: some spinel rims (Mg-Al-spinel) have been partially to completely replaced by hydrogarnet. All lavas contain variable proportions of secondary minerals such as serpentine, barite, witherite, and hydrogarnet.

Pyroclastic rocks

The pyroclastic rocks contain large rounded olivine xenocrysts (8–18 vol. %; Fig. 10A), which show large proportions of resorbed rims. The groundmass in juvenile pyroclasts is serpentine-poor (in comparison to the lavas) and contains larger apatite, perovskite and hydrogarnet grains (Fig. 9H). Serpentine is mostly found replacing forsterite inclusions in titanomagnetite and in partial to complete replacement of olivine xenocrysts (pseudomorphs). Spinel grains are rare and some contain forsterite inclusions. The rims of most spinels have been partially replaced by hydrogarnet. The pore space in the rocks is filled predominantly by calcite (Fig. 10A and 9H) and minor dolomite (Fig. 9H).

Cosmogenic ^{3}He dating results

Helium concentrations and isotopic compositions are presented in Table 1. Exposure ages of all samples are calculated using the equations in Kurz et al. (1987) and assumes no correction is required for implanted or *in situ* radiogenic ^{4}He.A sea level high latitude production rate of 120 ± 9 atoms/g/year (Goehring et al. 2010) was scaled for altitude and latitude using factors of Dunai (2000). Sparse vegetation cover (trees and bushes) is present at all samples sites but has not been sufficient to require correction, and no depth correction or self-shielding corrections were necessary. Topographic shielding is significant (~30%) for sample IH52. Exposure ages range from 5.9–12.4ka (Table 1). The low concentration of cosmogenic ^{3}He has resulted in relatively large age uncertainties, in one case up to 70 %. The arithmetic mean of the exposure ages suggest that the Igwisi Hills volcanoes were erupted at 8.9 ± 2.7 ka (1σ, n = 4). However, IH15 and IH61 have probably experienced a small degree of erosion, which suggests that the slightly older ages determined for sample IH52 (11.2 ± 7.8 and 12.4 ± 4.8ka) are better estimates of the eruption age.

Palaeomagnetic results

All of the 29 specimens from the 17 samples subjected to palaeomagnetic analysis yielded well-defined components of magnetisation. After removal of a randomly oriented component of magnetisation by Af fields of 12mT or temperatures of 200°C a stable characteristic remanence was isolated in all specimens. We attribute the low-stability component to a viscous magnetisation acquired post-sampling. The characteristic remanence was well grouped in 22 specimens from 12 samples, yielding a mean declination of 357.6° and a mean inclination of 6.1° (k=23.9; α= 9.1°; Fig. 10). The 7 specimens that yield stable magnetisations with anomalous directions were characterised by abnormally high NRM intensities, and we suspect that those outcrops had been subjected to lightning strikes. The mean direction obtained from the bulk of the lava samples is very close to the expected present field direction of the Igwisi Hills (Fig. 11), and is consistent with a young age for the lava, both in term of the direction and polarity of the lava.

Post-emplacement changes to Igwisi Hills

The IHV are young landforms that have undergone weathering, alteration, cementation and erosion since emplacement. The pyroclastic rocks are cemented by calcite and exhibit an unusual weathering style interpreted as dissolution (carbonation) features similar to grikes in Karst landscapes (Dawson 1994). There is little evidence that material weathered from the volcanoes has been transported away by surface water and less-soluble components (olivine crystals, lithic clasts) weathered from the tuffs have accumulated on the flanks of the volcanoes. Studies of modern volcanic craters indicate that their rims recede rapidly following eruption and feed scree slopes along the crater wall base, before stabilising (e.g., Pirrung et al. 2008; see also White and Ross 2011). Crater walls of the 1977 Ukinrek maars receded by 20 m over 27 years (Pirrung et al. 2008). Scree slopes are generally absent along the interior crater wall for the NE volcano (Fig. 2) and we suggest that the NE volcano's crater rims have receded little (metres) since emplacement.

Discussion

Emplacement of pyroclastic rocks

Two phases of pyroclastic activity are recorded at each of the IHV (Fig. 12). The pyroclastic rocks that make up the tephra cones of the IHV share some broad characteristics including centimetre to decimetre-scale bedding defined by sharp to gradational variations in the abundances and grainsizes of lithic clasts, olivine crystals or juvenile clasts (Table 3, Fig. 4; Fig. 5E); well to very well sorted (σ_Φ = 0.75–2; following Cas and Wright, 1987), a framework-supported texture of coarse ash and lapilli-sized clasts and a general absence of fine ash (< 200μm; Fig. 5A–C). The lateral extent of many beds is not known due to poor exposure, but the absence of recognizable tractional structures (e.g., dune bedforms) or erosion features suggests that they are fall deposits. Although this cannot be proven in all cases, most beds are persistent across individual outcrops (metre-scale). The rapid vertical changes in grainsize, composition and abundance of coarse fragments over centimetres to decimetres suggest deposition from numerous small explosions. We infer that the pyroclastic accumulated from unsteady eruption plumes that resulted from numerous closely-spaced discrete explosions. Steady conditions are recorded by thick massive beds in the SW volcano (lithofacies mbL, Table 3).

Contacts between the pre-eruption substrate and oldest pyroclastic rocks at each volcano are not exposed and neither are deposits from the opening phases of the eruptions. The oldest exposed pyroclastic rocks at each volcano are enriched in lithic clasts (lithofacies blT/blL; Fig.4 and 5A, Table 3), suggesting that early phases involved a degree of vent erosion. The overlying pyroclastic deposits, which contain virtually no lithic clasts and which make up the bulk of the tephra cones, are inferred to record eruptions with little or no vent erosion.

The pyroclastic edifices of all three volcanoes are built higher on their west and northwest sides (Fig. 2). This is most marked in the central volcano and is consistent with fallout from small, weak

eruption plumes(1–4 km) that were sheared by the dominant south-easterly trade winds (~13 ms^{-1}). Asymmetry due to wind shearing of plumes is common in small pyroclastic cones (e.g., Porter 1972). Similar interpretations have been proposed to account for volcano asymmetry identical to that of the IHV shown by some young maars and tuff cones in northern Tanzania (Dawson and Powell 1969; Mattsson and Tripoli 2011).

Emplacement of lavas

All three IHV record late-stage effusion of small volumes of degassed kimberlite magma (Phase 3, Fig. 12) that fed dense to poorly vesicular (<15 vol. %) lavas that travelled short distances from their vents (Fig. 2). Walker (1973) demonstrated a correlation between lava effusion rate and lava length over a wide range of lava viscosities and substrate slope angles. Using Walker's empirical relationships as a guide, we can constrain the effusion rates of the IHV lavas to <1 m^3/s, which gives emplacement times of up to 2 days. The thicknesses and physical features of the IHV lavas suggest relatively high effective viscosities.

Kimberlite magmas with silica contents of <25 wt % (e.g., Mitchell 1986) are inferred to have low melt viscosities (0.1–1 Pa s, Sparks et al. 2006).Large olivine crystals are concentrated in the lower third of the NE lava flow, but do not appear to form a cumulate layer (the crystals are not touching, Fig. 7). This observation can be used to place a first-order lower limit on the viscosity of the lava by using Stoke's Law (e.g., Rowland and Walker 1988). The concentration of olivine crystals towards the base of the lava (Fig.7) could be interpreted as due to syn- and post-emplacement settling of crystals or the consequence of co-eruption of crystal-rich and crystal-poor with denser crystal-rich lava being emplaced at the base of the flow. We favour the latter explanation. The olivine crystals are not touching (Fig. 7) as would be expected if they had settled from an original uniform distribution and aggraded at the base. They also show imbrication, indicative of in situ orientation in a shear flow. The lack of settling within the basal crystal-rich 50 cm zone can be used to estimate a lower bound on viscosity. A time scale, t, can be constrained by the usual conductive scaling law in which $t \sim l^2/k$, where l is a characteristic length and k is the thermal diffusivity. Taking l = 0.25 m and a typical value of k = 6 x 10^{-7} m^2/s, a time scale of 28 hours (about 1 day) is calculated. Using Stokes law, a crystal diameter of 5 mm and a density contrast between olivine and surrounding melt of 500 kg/m^3, the viscosity for an olivine to sink 0.25 m in this time is approximately 2700 Pa s. This is not an exact threshold but if the viscosity had been much lower than this value then some settling and touching of olivine crystals might have been expected. Another explanation of the lack of settling is that the groundmass was partially crystallized or crystallising during emplacement, and evidence for this is provided by the flow-aligned groundmass calcite crystals. A partially crystallized groundmass can increase lava viscosity and also result in development of a yield strength (Castrucchio et al., 2010). From these considerations we infer that the lava has a viscosity likely around or above 10^3 Pa s. Additionally the nature of the residual melts during emplacement is not well constrained due to formation of abundant serpentine replacing unknown phases (Willcox et al., submitted).

The lava covering the eastern plateau of the NE volcano (Fig. 2) is inferred to overlie low-lying parts of the outward-dipping pyroclastic cone. The presence of lava >10 m above the crater floor suggests that the either crater must at some stage have been filled with lava up to this level, or that high-high-standing lava is clastogenic in origin, although we found no positive evidence for this (e.g., draping of crater walls or remnant pyroclastic textures in the lava). We interpret the lava on the eastern plateau to have been fed by overflows from a late-stage perched lava lake that filled the crater. We infer from flow directions given by olivine imbrication that this lava drained back into the crater. The present bowl-shaped crater is interpreted to have formed by subsidence of this lava lake. Withdrawal may have been caused by magma becoming diverted to a neighbouring volcano, by breaching of the pyroclastic cone around the NE volcano crater, or by some combination of both. Additionally,

compaction of the vent-filling pyroclastic material may have contributed to the subsidence of the crater floor (e.g., Lorenz 2007). Lava drain out through a cone breach is strengthened by the comparable volume estimates of the empty crater (1.9×10^5 m^3) and the flat-lying lava flow to the northeast (2×10^5 m^3), and by the presence of a prominent notch in the north crater walls (Fig. 2). We thus infer that the lava breached the pyroclastic cone in the NE of the crater and spread out across the ground. We interpret the stepped morphology along the inner eastern crater wall as the result of a series of partial circumferential faults, downthrown towards the crater, that were generated by subsidence following draining of the lava lake (Fig. 2). Lava does not outcrop along the northern and western walls of the crater, but we infer the tilted surface of this subsided lava lake underlies the shallow, inward-dipping slope in these parts (Fig. 2).

The lava of the central volcano is interpreted as a viscous lava coulée (Fig. 2). The presence of altered crustal inclusions (2.5–5.5 vol. %) dispersed through the lava is puzzling (Fig. 8). Mixing cold lithic clasts into lava is difficult. Similar lithic-bearing, igneous-textured layered rocks within other kimberlite pipes, in some cases at depths of >1 km have been interpreted as welded pyroclastic rocks that result from the mixing of fragmented lithic material and hot juvenile clasts within an explosive pyroclastic jet or fountain (e.g., Sparks et al. 2006; Brown et al. 2008a, 2009; van Straaten et al., 2011). Texturally similar rocks in basaltic volcanic systems have also been interpreted as welded pyroclastic rocks from weak inefficient fountains (McClintock et al., 2008). The morphology of the central volcano lava coulée seems incompatible with in-situ deposition from a fountain as there is no evidence for layering within the lava or for mantling of the adjacent cone by welded pyroclastic deposits. Either the lithic clasts were incorporated at depth, when the magma was at a low viscosity, or the coulée represents a densely welded pyroclastic rock that accumulated in the conduit and was subsequently extruded as a viscous plug. Biotite is stable in the altered basement xenoliths within the central volcano coulée and this constrains its emplacement temperature to below about 850°C (Douce and Beard 1994). The consistent palaeomagnetic directions indicate emplacement temperatures above the Curie temperature for groundmass titanomagnetite (550^{o}C).

Comparison with other small monogenetic volcanoes

The IHV are small volcanoes with minimum volumes of preserved surface volcanic products of ~10^6 m^3 (Table 2). The volumes of erupted material dispersed away from the volcanoes by ash clouds during the eruptions and removed from the volcanoes by erosion are not known, but accounting for this would mean that the IHV eruptions were probably at least VEI 2 in magnitude (>0.01 km^3, e.g., Newhall and Self 1982). This is typical for small monogenetic eruptions.

The well preserved nature of the IHV allows comparison with other types of monogenetic volcanoes (scoria cones, tuff rings, tuff cones and maars, see Wood 1980; Wohletz and Sheridan 1983; White and Ross 2011). The IVH have been eroded and comparisons based on edifice morphology need to be made with caution. Bedding dips in pyroclastic edifices of the IHV vary from 4–32° with mean dips of 18–21° (Fig. 2). These dips are lower than those typical of scoria cones (critical angle of repose, 30–35°), but are similar to those of small phreatomagmatic volcanoes (e.g., tuff rings, tuff cones and maars, White and Ross, 2011). The NE volcano resembles a small maar volcano or tuff ring with its ~200 m-wide crater sitting at or just below the palaeo-surface. It is small for a maar volcano, which have mean diameters in the range 340–550 m (Ross et al. 2011). The pyroclastic edifice of the central volcano is partly buried by later-erupted lava, but in terms of bedding dips, it compares to tuff cones. The SW volcano hasa well-developed cone morphology, dip angles mostly below the angle of repose and a perched crater, and morphologically resembles a tuff cone or scoria cone.

Tuff cones and maar volcanoes commonly show textural and physical evidence in both deposits and pyroclasts for explosive interaction with ground or surface water. This can lead to a suite of features that may include elevated quantities of lithic clasts in pyroclastic deposits (e.g., Fisher and

Schmincke 1984; Valentine2012), large ballistic lithic clasts, crudely bedded and stratified pyroclastic deposits, dense to poorly vesicular pyroclasts (e.g., Wohletz and Sheridan1983), fine ash layers and ash aggregates (e.g., accretionary lapilli), and edifices comprised of both pyroclastic density current deposits (less common in tuff cones) and pyroclastic fall deposits (see White and Ross 2011; Valentine, 2012). The IHV exhibit lithic-bearing crudely bedded pyroclastic deposits (lithofacies blT and blL, Table 3) and dense or poorly vesicular pyroclasts (Phase 1, Fig. 4 and 5A). Fine ash layers, ash aggregates and pyroclastic density current deposits were not observed (note: ash aggregates and pyroclastic density current deposits have been found in other kimberlite pipes, e.g., Venetia pipes, Kurszlaukis and Barnett 2003; Jwaneng pipes, Brown et al. 2008b; Orapa pipes, Gernon et al. 2009a; Porritt and Russell in press). Large ballistic lithic clasts are absent in the IHV even in ultra-proximal deposits. Clasts >5 cm in diameter are rare and clasts >10 cm in diameter are extremely rare at each IHV (e.g., Fig. 6F). Large juvenile bombs (>50 cm in diameter) also common in proximal settings during monogenetic eruptions are similarly absent in the IHV. The small juvenile pyroclast size (coarse ash to fine lapilli) probably reflects the explosive disruption of predominantly low viscosity magma: this is backed-up by the droplet shapes of many kimberlite pyroclasts (e.g., Mitchell 1986; Moss et al. 2011). The absence of large lithic ballistic clasts is puzzling, because even weak explosions eject coarse lithic clasts over proximal areas. One possibility is that explosions were occurring at depth in the conduits, and large clasts could not escape (e.g., Sparks et al. 2006). This remains to be explored as a possibility at the IHV. There is little preserved environmental evidence for surface water at the time of the IHV eruptions but it is possible that ephemeral surface water was present. The country rock comprises crystalline basement—potentially a poor aquifer for driving maar eruptions.

The IHV pyroclastic edifices share similarities with small cones formed by basaltic magmatic eruptions. The Phase 2 juvenile-rich pyroclastic deposits (e.g., lithofacies bL, bpelL, Table 3) contain very low volumes of lithic material, comparable to the volumes common in basaltic scoria cones (e.g., Valentine and Groves 2008; Valentine 2012). The crude bedding and stratification of the fall deposits of the IHV are compatible with fallout from unsteady eruption plumes. The SW volcano most closely resembles a scoria cone with a preserved crater width of W_{cr}=0.4W_{co} (cone width), comparable to scoria cones, but a cone height of H_{co}= 0.1W_{co}. The latter is half that expected for scoria cones (H_{co}=0.18W_{co}, Wood 1980).Mean bedding dips below the critical angle of repose may result from wind-sheared volcanic plumes blown towards the northwest by trade winds, or, given the small size of the IHV, from scoria cone-forming eruptions that aborted before pyroclasts had built up to the critical angle of repose (e.g., McGetchin et al. 1974). We infer that the effusive stages of the IHV represent eruptions driven by ascent of gas-poor magma toward the ends of the eruptions.

There are similarities between the IHV and small volcanoes in the Lake Natron-Engaruka monogenetic volcanic field, Northern Tanzania (Dawson and Powell 1969; Mattsson and Tripoli 2011). These volcanoes, which are olivine melilitite to nephelinite in composition, exhibit morphologies comparable to tuff rings, tuff cones, maars and scoria cones. Despite the similarities with small phreatomagmatic volcanoes, the pyroclastic deposits of the maar-type volcanoes exhibit textural evidence inferred to result from dry (i.e., not phreatomagmatic) fragmentation and deposition. Mattsson and Tripoli (2011) concluded that the eruptions may have instead been magmatic and driven by the high volatile contents of the melilititic melts. Similar arguments have been put forward for kimberlite eruptions (e.g., Sparks et al. 2006).

The deposits and volcanoes at Igwisi Hills thus share characteristics with both small phreatomagmatic volcanoes (bedding dips, a sunken crater and lithic-rich bedded pyroclastic deposits) and with scoria cones (juvenile-rich deposits, moderately poor to good sorting). Small monogenetic eruptions can be complex and flip between phreatomagmatic and magmatic activity. Early phreatomagmatic phases can exhaust surface or ground water or build edifices that block water access to the vent—later phases are magmatic (e.g., Phases 2 and 3 at the IHV). This is a scenario that would

fit the evidence at Igwisi, although we note that the deposits lack evidence for wet deposition and phreatomagmatic explosions (e.g., fine ash layers, ash aggregates, large ballistic blocks).

Comparison with ancient kimberlite volcanoes

The IVH are small in comparison to many well-studied kimberlite pipes, whose craters can exceed 500 m in diameter (e.g., Field and Scott-Smith 1999; Field et al. 2008). Few examples of the surface edifices of kimberlites volcanoes are known. The best documented are the Cretaceous Fort à la Corne kimberlites in Canada, which comprise pyroclastic cones and reworked volcaniclastic rocks emplaced in a coastal or submarine environment (e.g., Leckie et al. 1997; Berryman et al. 2004; Pittari et al. 2008Berryman et al. 2004). They are presently buried under thick glacial till. These volcanoes have been interpreted as either shallow, wide craters filled with pyroclastic rocks (Berryman et al. 2004), positive relief tephra cones and tuff rings (Leckie et al. 1997; Zonneveld et al. 2004; Kjarsgaard et al. 2007, 2009), or some combination of the two (Pittari et al. 2008; Lefebvre and Kurszlaukis 2008). Seismic reflection surveys of the 169 kimberlite appear to outline a cone 50–100 m high and >1 km in diameter (e.g., Kjarsgaard et al. 2007). The near-shore setting of these volcanoes and common presence of aqueously reworked volcaniclastic beds has led many authors to infer that the eruptions were in part phreatomagmatic (Kjarsgaard et al. 2007, 2009; Pittari et al. 2008; Lefebvre and Kurszlaukis 2008). Pyroclastic deposits include those inferred to be proximal and distal magmatic fall deposits, poorly sorted debris jet deposits from wet phreatomagmatic eruptions, and coarse-grained poorly sorted proximal pyroclastic flow deposits (Kjarsgaard et al. 2009).

The Meso-Neoproterozoic Tokapal kimberlite, India (Mainkar et al. 2004), comprises a 2 km wide apron of weathered and buried pyroclastic rocks 70 m thick around a large crater. The pyroclastic rocks comprise fine-grained tuffs, pyroclastic breccias with abundant lithic clasts and stratified lapilli-tuffs in which stratification is defined by lithic clast abundance. They are interpreted as pyroclastic density current deposits and pyroclastic fall deposits and appear to form an eroded low, broad tephra ring akin to a tuff ring. The Tokapal deposits overlie marine limestones and shales but may have been erupted subaerially following uplift (Mainkar et al. 2004).

The pyroclasts of the IHV pyroclastic rocks are morphologically similar to those found in the kimberlite tephra cones discussed above, in ancient kimberlite pipes (e.g., Mitchell 1986; Moss et al., 2011) and other ultrabasic volcanoes (e.g., kamafugite diatremes, Junqueira-Brod et al. 2004). For example, pyroclastic rocks of the Fort à la Corne kimberlites contain variable amounts of dense to poorly vesicular irregular-shaped clasts, pelletal clasts and free olivine crystals (e.g., Zonneveld et al. 2004; Lefebvre and Kurszlaukis 2008; Kjarsgaard et al. 2009). Spherical droplet-shaped and irregular-shaped pyroclasts (Fig. 5A and D) and pelletal clasts result from the disruption of low viscosity magma, while the angular and poorly vesicular juvenile clasts (Fig. 5B and C) suggest fragmentation of higher viscosity magma that had already undergone some degree of groundmass crystallization and glass formation.

Occurrences of kimberlite lavas are rare due to erosion and few have been documented (e.g., Mainkar et al. 2004; Skinner and Marsh 2004; Eley et al. 2008). Eley et al (2008) report intersections of igneous-textured kimberlite encountered at shallow levels in Angola. One body, which was also imaged by geophysical methods, was interpreted as a 200 m wide × 1000 m long, 3 m thick extra crater lava flow. The other was a >130 m thick coherent kimberlite unit interpreted as a lava lake. Rocks interpreted to be extra-crater lava flows at the Tokapal kimberlite, India, are heavily weathered and only encountered in drill core (Mainkar et al. 2004). Van Straaten et al (2011) interpreted a high-level body of igneous-textured kimberlite in the Victor pipe, Canada, as a lava lake. This supports our interpretation of lava lakes in the IHV.

Subsurface plumbing at the IHV

The dimensions of the IHV conduits and the volume of material contained within them remain largely unconstrained (Fig. 13). Surface crater radii of >50–100 m (Fig. 2) constrain the maximum diameters of any conduits, but the vertical extent and shape of the conduits (whether pipes or dikes) remains unknown. In ancient kimberlite pipes and other diatremes pipe walls are typically oriented inward at angles of 70–90°, with average dips of 82–85° inferred for kimberlite pipes (Hawthorne 1975; White and Ross 2011). Using these average values, hypothetical kimberlite pipes would extend 300–500 m beneath the central and SW volcanoes and 600–900 m beneath the NE volcano. This can be tested by estimating the minimum volume of excavated country rock obtained by calculating the volume of lithic clasts within the pyroclastic deposits. The oldest pyroclastic deposits contain the largest volumes of lithic clasts (Phase 1) and the general absence of lithic clasts in later products (Phases 2 and 3) indicates that subsurface conduits were not substantially enlarged after the early phase. The volume of these pyroclastic deposits is not well constrained, but for the NE Volcano, generously assuming that they originally formed a circular apron that was 10 m thick at the crater edge and that thinned to zero at 300 m distance, then the tuffs have a minimum volume of 2×10^6 m^3. If basement clasts account for on average 15 vol. % of the deposits, then the minimum volume of excavated country rock is 3×10^5 m^3. This volume is roughly equivalent to either a cone with a radius of 50 m and a depth of ~110 m, or a 3 m widening of a dike segment 200 m long and 500 m deep. This calculation assumes that large volumes of fragmented country rock were not dispersed widely during the eruption and do not remain trapped in the conduit. Comparisons with other kimberlite pipes suggest that the trapped volume should account for <<50 vol. % of a pipe's volume (Sparks et al., 2006). These first order estimates of excavated country rock do not imply that there are substantial conduits beneath the IHV Volcano. Although deposits of the opening phases of the eruptions are not exposed, the absence of granite-rich pyroclastic breccias mantling deposits of older, neighbouring volcanoes suggests that any explosive cratering (e.g., Sparks et al., 2006) was minimal at the IHV. These estimates suggest small conduits comparable in dimensions to those beneath scoria cones (e.g., Doubik and Hill, 1999; Keating et al. 2008; Valentine 2012; Fig. 13). Future research at Igwisi should combine geophysical studies (resistivity, gravity and magnetic surveys) with rock drilling to constrain the subsurface plumbing system.

Duration of IHV eruptions

Minimum erupted volumes of ~10^6 m^3 for the IHV are at the lower end of estimates based on pipe volumes for kimberlite eruptions (Sparks et al. 2006) and are consistent with their small crater diameters and edifice dimensions. We infer that the IHV were formed by small volume, monogenetic eruptions of kimberlitic magma that ascended along a NE–SW oriented dike(s) (Fig. 13). The eruptions probably persisted for several days up to several months (comparable to monogenetic basaltic eruptions) and concluded with effusive phases that each lasted for several hours to days.

Conclusions

The three Igwisi Hills volcanoes, Tanzania, are the only examples of kimberlite volcanoes that still have surface constructs preserved on the Earth's surface. Cosmogenic ^{3}He exposure dating of olivine in the lavas gives Upper Pleistocene/Holocene eruption ages. This age is supported by palaeomagnetic analyses and confirms them as the youngest known kimberlite bodies. Such young eruption ages may indicate that the Tanzanian craton is undergoing a new phase of kimberlitic volcanism and more eruptions of kimberlitic magma may be expected in the future. The three small volcanoes comprise pyroclastic edifices, craters and lavas and were generated by small-volume (VEI 2), monogenetic eruptions of kimberlite magma that reached the Earth's surface along a NE–SW-oriented dike or dikes (Fig. 13). The pyroclastic cones are comprised of diffusely bedded fall deposits and pyroclasts include vesicular scoriaceous clasts, pelletal clasts and dense juvenile clasts. Bedding and pyroclast

characteristics are consistent with repetitive small explosions. Pyroclasts are similar in size and morphology to those commonly found in other kimberlite rocks indicating overlap in magma fragmentation dynamics between the Igwisi eruptions and those recorded by ancient kimberlite pipes. The morphology and physical features of the lavas indicate unexpectedly high lava viscosity, probably as a result of degassing and partial groundmass crystallization of the magma at shallow depth. Each volcano broadly shows the same three eruptive phases: 1) early vent-clearing explosive eruptions comprising elevated quantities of fragmented country rock, and that may have been drive by phreatomagmatic explosions; 2) lower-intensity juvenile-rich explosive eruptions that generated weak eruption columns that were sheared by dominant trade winds from the east and south-east (Fig. 13), and that constructed pyroclastic edifices around the vents and; 3) waning-stage effusions of degassed and partially crystallised viscous lava. These are comparable to eruption pathways observed at, and inferred for, many eruptions of other types of magmas.

Acknowledgements

We dedicate this paper to Barry Dawson—the last geologist to visit the volcanoes in 1966—as thanks for his great encouragement, advice and help and for many fruitful discussions throughout this study. Field and laboratory studies were supported a National Geographic Committee on Research and Exploration grant (no. 8562_08) awarded to RJB, the Natural Environment Research Council Geophysical Equipment Facility (grant no. 894) and the Royal Society International Travel Grant scheme. RSJS acknowledges support from a European Research Council Advanced grant. Alan Hobbs and Colin Kay at GEF are thanked for training and support. We thank Craig Storey and Dan Condon for advice on radiometric dating. We are indebted to Rod Smith of Cranbrook School, Kent, Mama Kisinga and the Friends of Urambo and Mwanhala charity for logistical support, lodgings, help and advice. We thank Urambo district council and the villagers at Igwisi for permission to work at the volcanoes. Bruce Kjarsgaard, Pierre-Simon Ross and Greg Valentine are thanked for expert reviews that greatly improved the manuscript. James White is thanked for editorial input and discussion.

References

Bassett H (1954). The Igwisi craters and lavas. Rec Geol Surv Tanganyika 4:81–92.

Batumike JM, Griffin, WL, Belousova NJ, Pearson NJ, O'Reilly SY, Shee SR (2008). LAM-ICPMS U-Pb dating of kimberlitic perovskite: Eocene–Oligocene kimberlites from the Kundelungu Plateau, D.R. Congo. Earth Planet Sci Lett 267:609–619.

Bell K, Dodson MH (1981).The geochronology of the Tanzanian shield. J Geol 89:109–128.

Berryman A, Scott Smith BH, Jellicoe B (2004). Geology and diamond distribution of the 140/141 kimberlite, Fort à la Corne, central Saskatchewan, Canada. Lithos 76:99–114.

Brown RJ, Buse B, Sparks RSJ, Field M (2008a). On the welding of pyroclasts from very low–viscosity magmas: Examples from kimberlite volcanoes. J Geol116:354–374.

Brown RJ, Gernon T, Steifenhofer, Field M (2008b). Geological constraints on the eruption of the Jwaneng central kimberlite pipe, Botswana. JVolcanolGeothermRes174:195–208.

Brown RJ, Tait M, Field M, Sparks RSJ (2009). Geology of a complex kimberlite pipe (K2 pipe, Venetia mine, South Africa): Insights into conduit processes during explosive ultrabasic eruptions. Bull Volcanol 71:95–112.

Buisman I, Sparks RSJ, Manya S, Brown RJ, Kavanagh J, Walter MJ, submitted. Olivine chemistry of exceptionally young (Holocene) kimberlite of the IHV, Tanzania. Contrib Min Pet.

Buse B, Schumacher JC, Sparks RSJ, Field M (2010).Growth of bultfonteinite and hydrogarnet in metasomatized basalt xenoliths in the B/K9 kimberlite, Damtshaa, Botswana: insights into hydrothermal metamorphism in kimberlite pipes. Contrib Min Pet 160:533–550.

Cas RAF, Wright JV (1987). Volcanic Successions. Chapman and Hall, London p. 528.

Cas RAF, Hayman P, Pittari A, Porritt L (2008). Some major problems with existing models and terminology associated with kimberlite pipes from a volcanological perspective, and some suggestions. J Volcanol Geotherm Res 174:209–225.

Castrucchio A, Rust A, Sparks RSJ (2010). Rheology and flow of crystal-rich bearing lavas: insights from analogue gravity currents. Earth Planet Sci Lett 297:471-480.

Davis GL (1977).The ages and uranium contents of zircons from kimberlites and associated rocks. Carnegie Institute Washington. 76:631–635.

Dawson JB (1964). Carbonate tuff cones in northern Tanganyika. Geol Mag 101:129–137.

Dawson JB (1971).Advances in Kimberlite Geology. Earth Sci Rev 7:187–214.

Dawson JB (1994).Quaternary kimberlitic volcanism on the Tanzania craton. Contrib Min Pet 116:473–485.

Dawson JB, Powell DG (1969). The Natron-Engaruka explosion crater area, Northern Tanzania, Bull. volcanol.33:761–817.

Dawson JB, Hawthorne JB (1973).Magmatic sedimentation and carbonatitic differentiation in kimberlite sills at Benfontein, South Africa. J Geol Soc London 129:61–85.

Doubik P, Hill BE (1999). Magmatic and hydromagmatic conduit development during the1975 Tolbachik Eruption, Kamchatka, with implications for hazards assessment at Yucca Mountain, NV.J Volcanol Geotherm Res 91:43-64.

Douce AEP, Beard JS (1994). Dehydration melting of biotite gneiss and quartz amphibolite from 3 to 15 kbar. J Pet 36:707–738.

Dunai TJ (2000). Scaling factors for production rates of in situ produced cosmogenic nuclides: a critical reevaluation. Earth Planet Sci Lett 176:157–169.

Eley R, Grütter H, Louw A, Tunguno C, Twidale J (2008). Exploration Geology of the Luxinga Kimberlite Cluster (Angola) with Evidence Supporting the Presence of Kimberlite Lava. Extended Abstract 9th Int. Kimberlite Conf.

765 Field M, Gibson JG, Wilkes TA, Gababotse J, Khutjwe P (1997). The geology of the Orapa A/K1
766 Kimberlite, Botswana: further insight into the emplacement of kimberlite pipes. In: Dobretsov NL,
767 Goldin SV, Kontorovich AE, Polyakov GV, Sobolev NV (Eds), Proceedings of the Sixth International
768 Kimberlite Conference 1: Kimberlites, Related Rocks and Mantle Xenoliths. Russian Geology and
769 Geophysics, Novosibirsk, Russia, 24–39.
770
771 Field M, Scott Smith BH (1999). Contrasting geology and near–surface emplacement of kimberlite
772 pipes in southern Africa and Canada. In: Gurney, J., Gurney, J., Pascoe, M., Richardson, S. (Eds.), J.B.
773 Dawson Volume. Proceedings of the VIIth International Kimberlite Conference. Vol. 1. Red Roof
774 design cc, Cape Town 214–237.
775
776 Field M, Stiefenhofer J, Robey J, Kurszlaukis S (2008). The kimberlite–hosted diamond deposits of
777 southern Africa: a review. Ore Geology Reviews 34:33–75.
778
779 Fisher RV, Schmincke H-U (1984). Pyroclastic Rocks. Springer-Verlag, Berlin, New York, 1984.
780
781 Foeken JPT, Persano C, Stuart FM, ter Voorde M. (2007). Role of topography in isotherm perturbation:
782 Apatite (U-Th)/He and fission track results from the Malta tunnel, Tauern window, Austria. Tectonics
783 26.
784
785 Fontana GPG, Mac Niocaill C, Brown RJ, Sparks RSJ, Field M (2011). Emplacement temperatures of
786 pyroclastic and volcaniclastic deposits in kimberlite pipes in southern Africa. Bull Volcanol 73:1063–
787 83
788
789 Fozzard PMH (1956). Further notes on the volcanic rocks from Igwisi, Tanganyika. Rec Geol Surv
790 Tanganyika, 6:69–75.
791
792 Gernon T, Gilbertson M, Sparks RSJ, Field M (2008a). Gas-fluidisation in an experimental tapered
793 bed: Insights into processes in diverging volcanic conduits. J Volcanol Geotherm Res 174:49–56.
794
795 Gernon T, Sparks RSJ, Field M (2008b). Degassing structures in volcaniclastic kimberlite: examples
796 from southern African pipes. J Volcanol Geotherm Res 174:186–194.
797
798 Gernon TM, Fontana G, Field M, Sparks RSJ, Brown RJ, Mac Niocaill C (2009a). Pyroclastic flow
799 deposits from a kimberlite eruption: the Orapa south crater, Botswana. Lithos, 112:566–578.
800
801 Gernon TM, Fontana G, Field M, Sparks RSJ (2009b). Depositional processes in a kimberlite crater:
802 the Upper Cretaceous Orapa South Pipe (Botswana). Sedimentology 56:623–643.
803
804 Gobba JM (1989). Kimberlite exploration in Tanzania. J African Earth Sci 9 314:565–578.
805
806 Goehring BM, Kurz MD, Balco G, Schaefer JM, Licciardi J, Lifton NA (2010). Reevaluation of in situ
807 cosmogenic (3)He production rates. Quat Geochron 5:410–418.
808
809 Haggerty SE, Raber E, Naeser CW (1983). Fission track dating of kimberlite zircons. Earth and
810 Planetary Science Letters 63: 41–50.
811
812 Hawthorne JB (1975).Model of a kimberlite pipe. Phys Chem Earth 9:1–15

Hon K, Kauahikaua J, Denlinger R, Mackay K (1994).Emplacement and inflation of pāhoehoe sheet flows: observations and measurements of active lava flows on Kilauea volcano, Hawai´i. Geol Soc Am Bull106:351–370

Junqueira–Brod TC, Brod JA, Gaspar JC, Jost H (2004). Kamafugitic diatremes: Facies characterisation and genesis—examples from the Goiás alkaline province, Brazil. Lithos 76:261–282.

Keating GN, Valentine GA, Krier DJ, Perry FV (2008) Shallow plumbing systems for small-volume basaltic volcanoes. Bull Volcanol 70:563–582.

Kjarsgaard BA (2007). Kimberlite diamond deposits, in Goodfellow WD, Ed, Mineral Deposits of Canada: A Synthesis of Major Deposit Types, District Metallogeny, the Evolution of Geological Provinces, and Exploration Methods: Geological Association of Canada, Mineral Deposits Division, Special Publication 5:245–272.

Kjarsgaard BA, Leckie DA, Zonneveld J–P (2007). Discussion of "Geology and diamond distribution of the 140/141 kimberlite, Fort à la Corne, central Saskatchewan, Canada" by Berryman AK, Scott Smith BH, Jellicoe BC (Lithos76:99–114). Lithos 97:422–428.

Kjarsgaard BA, Harvey S, McClintock M, Zonneveld JP, Du Plessis P, McNeil D, Heaman L (2009). Geology of the Orion South kimberlite, Fort à la Corne, Canada. Lithos 1125:600–617.

Kurszlaukis S, Barnett WP (2003) Volcanological and structural aspects of the Venetia Kimberlite cluster – a case study of South African kimberlite maar-diatreme volcanoes South African J Earth Sci 106: 165–192.

Kurszlaukis S, Lorenz V (2008). Formation of "Tuffisitic Kimberlite" by phreatomagmatic processes. J Volcanol Geotherm Res 174:68–80.

Kurz MD, Colodner D, Trull TW, Sampson DE (1987).Exposure age dating with cosmogenic ^{3}He: Influence of the Earth's magnetic field. EOS, 68:1286.

Leckie DA, Kjarsgaard BA, Bloch J, McIntyre D, McNeil D, Stasiuk L, Heaman L (1997). Emplacement and reworking of Cretaceous, diamond-bearing, crater facies kimberlite of central Saskatchewan, Canada. Geol Soc Am Bull 109:1000–1020.

Lefebvre N, Kurszlaukis S (2008). Contrasting eruption styles of the 147 kimberlite, Fort à la Corne, Saskatchewan, Canada. J Volcanol Geotherm Res 174:171–185.

Lipman PW, Banks NG (1987).´A´ā flow dynamics, Mauna Loa 1984. US Geol Surv Prof Paper 1350:1527–1567

Lorenz V (1975). Formation of phreatomagmatic maar-diatreme volcanoes and its relevance to kimberlite diatremes. Phys. Chem. Earth 9:17–27.

Lorenz V (2007). Syn- and post-eruptive hazards of maar-diatreme volcanoes. J Volcanol Geotherm Res 159:285-312.

Lorenz V, Kurszlaukis S (2007). Root zone processes in the phreatomagmatic pipe emplacement model and consequences for the evolution of maar-diatreme volcanoes. J Volcanol Geotherm Res 159:4–32.

Macdonald GA (1953).Pāhoehoe, ´a´ā and block lava. Am J Sci 215:169–191

Mainkar D, Lehmann B, Haggerty SE (2004). The crater–facies kimberlite system of Tokapal, Bastar district, Chhattisgarh, India. Lithos, 76:201–217.

Mattsson HB, Tripoli BA (2011).Depositional characteristics and volcanic landforms in the lake Natron-Engaruka monogenetic field, northern Tanzania. J Volcanol Geotherm Res 203:23–34.

McClintock M, White JDL, Houghton BF, Skilling IP (2008). Physical volcanology of a large crater-complex formed during the initial stages of Karoo flood basalt volcanism, Sterkspruit, Eastern Cape, South Africa. J Volcanol Geotherm Res 172:93-111.

McGetchin TR, Settle M, Chouet BA (1974). Cinder Cone Growth Modeled After Northeast Crater, Mount Etna, Sicily. J Geophys Res 79:3257-3272.

Mitchell RH (1970). Kimberlite and related rocks – a critical reappraisal. J Geol 78:686–704.

Mitchell RH (1986). Kimberlites. Mineralogy, Geochemistry and Petrology. Plenum Press 442p.

Mitchell RH (2008). Petrology of hypabyssal kimberlites: relevance to primary magma compositions. J Volcanol Geotherm Res 174:1–8.

Moss S, Russell JK, Andrews GDM (2008) Progressive infilling of a kimberlite pipe at Diavik, Northwest Territories, Canada: Insights from volcanic facies architecture, textures, and granulometry. J Volcanol Geotherm Res 174:103-116.

Moss S, Russell JK (2011). Fragmentation in kimberlite: products and intensity of explosive eruptions. Bull Volcanol72:983–1003.

Newhall CG, Self S (1982). The volcanic explosivity index (VEI): An estimate of explosive magnitude for historical volcanism. J Geophys Res 87:123–1238.

Pirrung M, Büchel G, Lorenz V, Treutler H- (2008). Post–eruptive development of the Ukinrek east maar since its eruption in 1977 A.D. in the periglacial area of south–west Alaska. Sedimentology 55: 305–334.

Pittari A, Cas RAF, Lefebvre N, Robey J, Kurszlaukis S, Webb K (2006). Eruption processes and facies architecture of the Orion central kimberlite volcanic complex, Fort a la Corne, Saskatchewan; kimberlite mass flow deposits in a sedimentary basin. J Volcanol Geotherm Res 174:152–170.

Porritt LA, Cas R, Crawford BB (2008). In-vent column collapse as an alternative model for massive volcaniclastic kimberlite emplacement: an example from the Fox kimberlite, Ekati Diamond Mine, NWT, Canada. J Volcanol Geotherm Res 174:90–102.

Porritt LA, Russell JK (in press). Kimberlite ash: fact or fiction? Phys Chem Earth.

Porter SC (1972). Distribution, Morphology, and Size Frequency of Cinder Cones on Mauna Kea Volcano, Hawaii. Geol Soc Am Bull 83:3607-3612.

Reid AM, Donaldson CH, Dawson JB, Brown RW, Ridley WI (1975). The Igwisi Hills extrusive "kimberlites". Phys Chem Earth 9:199–218.

Ross P–S, White JD (2006). Debris jets in continental phreatomagmatic volcano: A field study of their subterranean rocks in the Coombs Hills vent complex, Antarctica. J Volcanol Geotherm Res 149:62–84.

Ross P–S, Delpit S, Haller MJ, Németh K, Corbella H (2011). Influence of the substrate on maar-diatreme volcanoes—an example of a mixed setting from the Pali Aike volcanic field, Argentina. J Volcanol Geotherm Res 201:253–271.

Rowland SK, Walker GPL (1988).Mafic-crystal distributions, viscosities, and lava structures of some Hawaiian lava flows. J Volcanol Geotherm Res 35:55–66.

Sampson DN (1953). The volcanic hills at Igwisi. Rec Geol Surv Tanganyika 3:48–53.

Skinner EMW, Marsh JS (2004).Distinct kimberlite pipe classes with contrasting eruption processes. Lithos 76:183-200.

Sparks RSJ, Baker L, Brown RJ, Field M, Schumacher J, Stripp G (2006).Dynamical constraints on kimberlite volcanism. J Volcanol Geotherm Res 155:18–48.

Stiefenhofer J, Farrow DJ (2004). Geology of the Mwadui kimberlite, Shinyanga district, Tanzania. Lithos, 76:139–160.

Stripp GR, Field M, Schumacher JC, Sparks RSJ (2006).Post-emplacement serpentinization and related hydrothermal metamorphism in a kimberlite from Venetia, South Africa. J Met Geology 24: 515–534

Valentine GA (2012). Shallow plumbing systems for small-volume basaltic volcanoes, 2: evidence from crustal xenoliths at scoria cones and maars. J Volcanol Geotherm Res.

Valentine GA, Groves KR (2008). Entrainment of country rock during basaltic eruptions of the Lucero volcanic field, New Mexico. J Geol 104:71–90.

Van Straaten BI, Kopylova MG, Russell JK, Scott Smith BH (2011). A rare occurrence of a crater-filling clastogenic extrusive coherent kimberlite, Victor Northwest (Ontario, Canada). Bull Volcanol 73:1047–1062.

Walker GPL(1973).Lengths of lava flows. Phil Trans Roy Soc London. 274:107–118.

Walker GPL(1991).Structure, and origin by injection of lava under surface crust, of tumuli, "lava rises", "lava-rise pits", and "lava-inflation clefts" in Hawaii. Bull Volcanol53: 546–558.

Walters AL, Phillips JC, Brown RJ, Field M, Gernon T, Stripp G(2006). The role of fluidisation in the formation of volcaniclastic kimberlite: Grain size observations and experimental investigation. J Volcanol Geotherm Res 155:119–137.

White JDL, Houghton BF (2006). Primary volcaniclastic rocks. Geology 34:677–680.

White JDL, Ross P–S(2011). Maar-diatreme volcanoes: A review. J Volcanol Geotherm Res 201:1–29.

Willcox A, Buisman I, Sparks RSJ, Brown RJ, Manya S, Schumacher JS, Tuffen H (submitted). Petrology, geochemistry and low-temperature alteration of extrusive lavas and pyroclastic rocks of the Igwisi Hills kimberlites, Tanzania. Chem Geol.

Williams AJ, Stuart FM, Day SJ, Phillips WM (2005).Using pyroxene microphenocrysts to determine cosmogenic ^{3}He concentrations in old volcanic rocks: an example of landscape development in central Gran Canaria. Quat Sci Rev 24:211–222.

Wohletz KH, Sheridan MF (1983). Hydrovolcanic explosions II. Evolution of basaltic tuff rings and tuff cones. Am J Sci 283:385–413.

Wood CA (1980). Morphometric evolution of cinder cones. J Volcanol Geotherm Res7:387–413.

Zonneveld J-P, Kjarsgaard BA, Harvey SE, Heaman LM, McNeil DH, Marcia KY (2004). Sedimentologic and stratigraphic constraints on the emplacement of the Star kimberlite east–central Saskatchewan. Lithos 76:115–138.

Figure captions

Figure 1. Geological sketch map of the Tanzanian Craton. The IHV (4°53’19.22”S, 31°55’59.15”E) are situated on the western side of the craton, northwest of the village of Igwisi.

Figure 2. Geological and topographic map of the IHV. Insets show histograms of beddings dips in pyroclastic edifices and profiles of the three volcanoes.

Figure 3. Photographs of the three volcanoes. A) Cosmogenic sample site for IH15 (top of lava in NE volcano). B) Cosmogenic sampling site for IH52 (foot wall scarp in NE volcano lava developed during magma late-stage crater subsidence). C) The NE volcano, showing the flat crater floor, the northern crater wall comprised of pyroclastic rocks, and the lavas on the eastern side. View looking north from the central volcano. D) Central volcano showing the partial pyroclastic cone on the west of the volcano and the lava coulee that fills the inferred central volcano crater and has partially filled the NE volcano’s crater. View looking south from the northern margin of the NE volcano. E) The SW volcano showing the pyroclastic cone and central crater. The western side of the cone is 12 m higher than the eastern side. View towards the south from the central volcano.

Figure 4. Graphic summary log through pyroclastic deposits of the northern crater wall of the NE volcano. Photographs show: A) centimeter-scale bedding defined by variations in abundance of lithic clasts; B) close-up of A showing lithic lapilli of basement granite and gneiss; C) Close up of A showing clast-supported nature of juvenile and lithic lapilli.

Figure 5. Transmitted light thin-section photographs of pyroclastic lithofacies of the IHV (see Table 3). A) Lithic-bearing lapillistone (blL) from the NE volcano. Accidental clasts comprise crystals and rock fragments derived from the basement. ~50 cm shown on rule. Dense juvenile lapilli have amoeboid outlines or are pelletal lapilli. B) Juvenile-rich lapillistone comprised of poorly vesicular lapilli and ash-grade juvenile clasts with irregular outlines (central volcano). C) Close-up of vesicular juvenile lapilli in B. D) Extracted pelletal lapilli from the pelletal-clast-rich lapillistone shown in Figure 4C. E) Centimetre-scale stratification within juvenile-rich lapillistone and tuffs from the SW volcano. Comprised predominantly of amoeboid dense to poorly vesicular juvenile clasts.

Figure 6. Juvenile-rich pyroclastic lithofacies of the IHV (see Table 3). A) Coarse-grained scoria fall deposit (bL) overlain by coarse tuff. Centimetre divisions on rule. B) weakly bedded juvenile rich pyroclastic (bL) on inner crater wall of central volcano. 10 cm divisions on metre-rule. C) Bedded juvenile-rich lapillistone with scattered dense juvenile coarse lapilli. Centimetre divisions on rule. D) Close-up of bedded juvenile-rich lapillistone in d. Bedding is defined by grainsize. E) Rare lithic block in juvenile-rich lapillistone, central volcano. 10 cm divisions on rule. F) Bedded pelletal-clast-rich lapillistone (bpelL) from the NE volcano. Rock is comprised predominantly of clast-supported pelletal lapilli.

Figure 7. Graphic summary log (left) and photographs of polished slabs (centre) up through the lava flow of the NE volcano. Olivine crystals are concentrated in the lower third and vesicles are restricted to the upper third. Transmitted light photographs of thin-sections through the lava (right).

Figure 8. The lava coulee of the central volcano. A) Outcrop photo showing several lapilli-sized lithic clasts (granitic basement). B) Polished slab showing abundant ash-grade lithic clasts (light) and olivine crystals (dark).

Figure 9. Selected BSE images of various minerals found in IHV samples. A) Rounded xenocrystic olivine mantled with perovskite and Mg-Al-spinel. B) Marginally resorbed phenocrystic olivine found in the groundmass, C) Forsterite inclusion in a titanomagnetite host crystal, D) K-phlogopite with Ba-rich-phlogopite (kinoshitalite) overgrowths, E) Apatite hopper crystals and monticellite, F)Titanomagnetite with Cr-rich core and the Mg-Al-spinel rim replaced by hydrogarnet, G) Spongy tabular calcite laths and amorphous calcite including a spinel pseudomorph, H) Calcite with dolomitic patches found in tuff samples and sub-rounded apatite grains. Abbreviations: *fo* forsterite, *prv* perovskite, *sp* spinel, *t-sp* titanomagnetite, *cal* calcite, *dol* dolomite, *phg* phlogopite, *hgt* hydrogarnet, *mnt* monticellite, *ap* apatite, *srp* serpentine, *phenol* phenocryst, *xeno* xenocryst, Scale bars shown are 100 µm.

Figure 10. Selected BSE images of the groundmass mineralogy found in IHV samples. Refer to text for details. A) IH5, a tuff sample from the central volcano; B) IH20, a lava sample from the central volcano; C) IH30, top of NE lava flow; D) IH53, lower part of NE lava flow. Abbreviations found in caption for Figure 8. Scale bars all 100 µm

Figure11. Representative orthogonal plots of thermal demagnetisation (sample PL11a) and alternating field demagnetisation (sample PL4b) and an equal-area stereographic projection of sample-mean directions. In the orthogonal plots solid (open) circles represent projections into the horizontal (vertical) planes. On the stereographic projection the closed (open) symbols represent downward (upward) directed vectors. The mean direction is marked by a cross along with cone of 95% confidence about the mean.

Figure 12. Graphic summary log showing the deposits of the three main eruption phases that characterized the IVH eruptions.

Figure 13. Cross-sections of the IHV showing inferred structure of subsurface conduits as reconstructed from surface deposits. Insets show strong shearing of the volcanic plumes by trade winds and inferred position of NE-SW oriented dikes and craters (at pre-eruptive substrate level) for the three volcanoes. Position of cross-sections is shown. See Figure 2 for lithological key.

Sample	$^{3}He/^{4}He$ crush (R/R_a)	Melt weight (mg)	$^{3}He/^{4}He$ melt (R/R_a)	^{3}He cos* (10^5 atoms/g)	P local (atoms/g/yr)	Topographic shielding	Exposure age (ka)

IH15	4.59 ± 0.06	220	4.71 ± 0.13	7.9 ± 5.7	141	0.97	5.9 ± 4.3
IH52a	4.61 ± 0.04	209	10.2 ± 7.0	10.2 ± 7.0	141	0.65	11.2 ± 7.8
IH52b	4.61 ± 0.04	191	4.82 ± 0.06	11.4 ± 4.3	141	0.65	12.4 ± 4.8
IH61	4.53 ± 0.04	198	4.73 ± 0.06	10.1 ± 3.6	141	0.96	7.6 ± 2.8

Table 1. Results of ^{3}He cosmogenic dating of IHV lavas. IH15 is from the central volcano, all others are from the NE volcano.

	Volume (m^3)		
	Lava	**Pyroclastic**	**Total**
NE volcano	377 000	>795 000	1 172 000

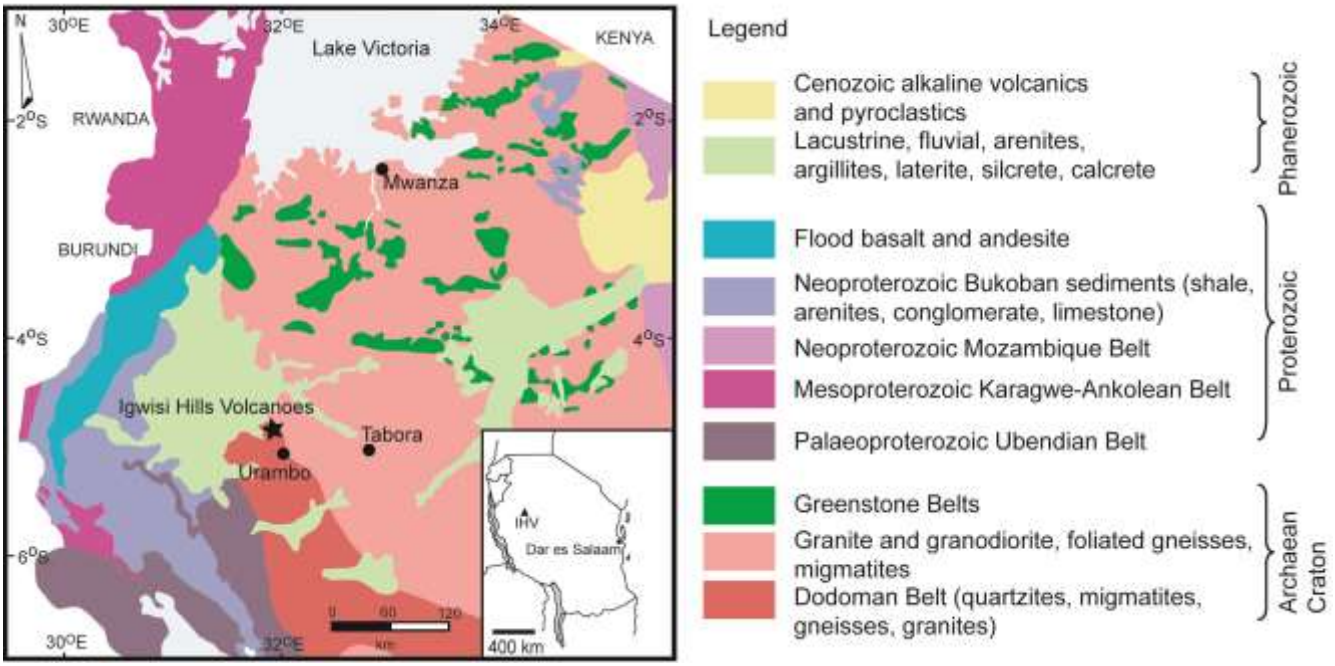
CE volcano	399 000	>910 000	1 309 000
SW volcano	>20 000	>995 000	1 015000
Total			3496 000

Table 2. Calculated volumes for preserved surface products of the IHV using xyz GPS survey data and Gemcom GEMS™ software.

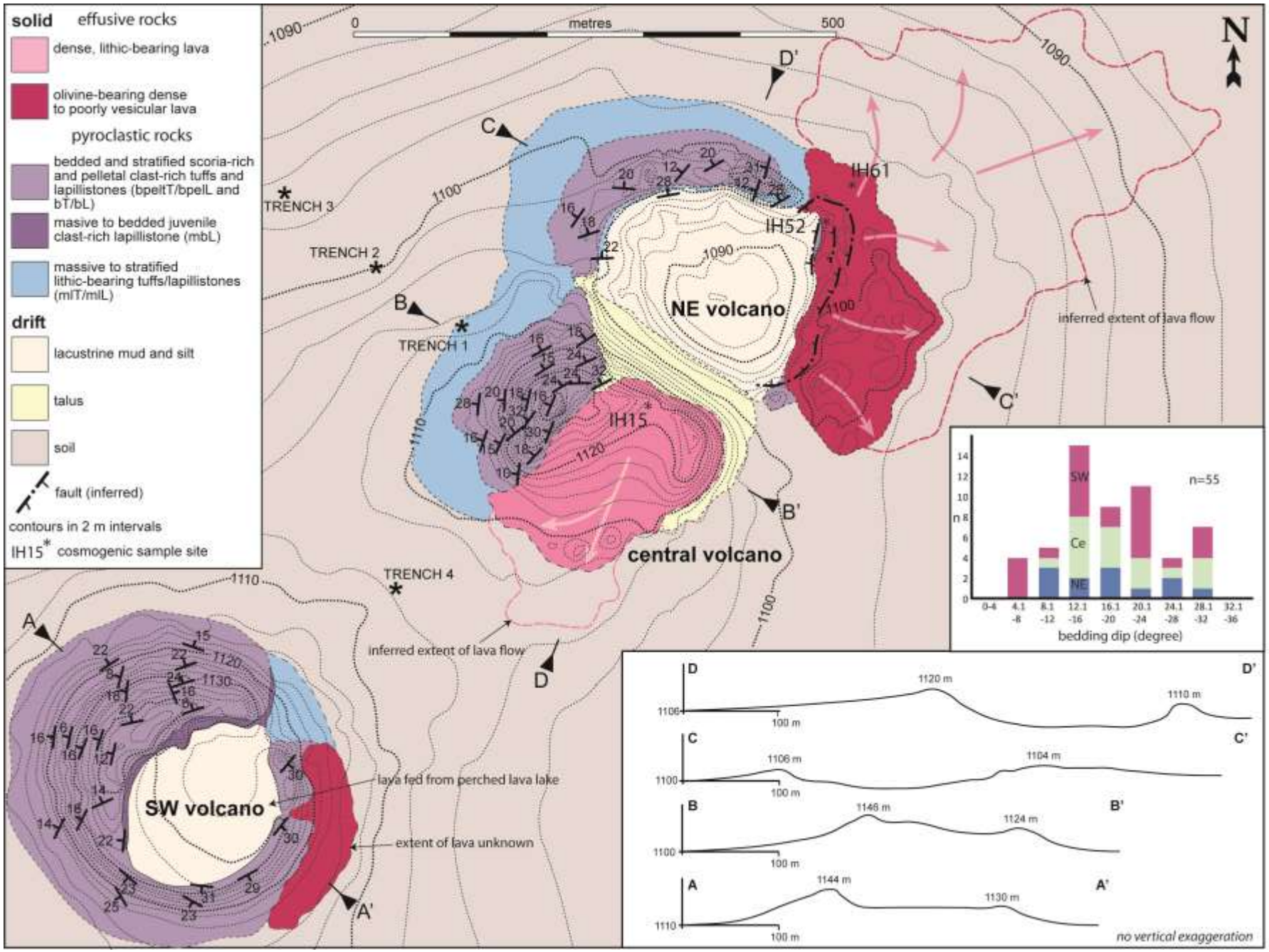
Lithofacies	Composition	Structure
Bedded lithic-bearing coarse tuff and lapillistone (blT/blL) See Figure 4.	Clast-supported, well sorted (σ_Φ= 2), coarse ash-and fine lapilli-grade olivine crystals, micro-xenoliths, juvenile clasts, pelletal clasts, lithic clasts and xenocrysts; non-vesicular juvenile clasts have irregular, amoeboid and spherical shapes and reach 4 mm in diameter; pelletal lapilli consist of olivine/micro-xenolith grains 0.2–2mm in diameter covered in a 0.01–0.5 mm thick coating of solidified kimberlite	Beds 2–25 cm thick; thinly bedded packages up to 1.6 m thick; defined by grainsize and abundance of lithic clasts and olivine

	groundmass; lithic clasts (<10cm diameter) present in low abundances (5–12 vol.%), rarely reaching ~40 vol.% and comprise ash to lapilli-sized granite and amphibolite lithic clasts and crustal xenocrysts with tabular to equant shapes.	crystals/micro-xenoliths.
Bedded pelletal clast-rich tuff and lapillistone (bpelT/bpelL) See Figure 6.	Clast-supported, very well sorted (σ_Φ= 0.75–1), subspherical pelletal clasts (30–60 vol. %) and juvenile clasts (40–70 vol. %) 0.25–8 mm in diameter; pelletal clasts (as above); juvenile clasts are dense to poorly vesicular with subspherical to weakly amoeboid shapes; vesicles are spherical to elongate and coalesced,0.01–0.5 mm in diameter and account for 5–11 vol. % of each clast; dense subspherical aphyric juvenile lapilli up to 5 cm in diameter account for <2–5 vol. % of this lithofacies.	Beds 0.5–15 cm thick; defined by sharp changes in grainsize; commonly occurs interstratified with bsT/bsL.
Bedded juvenile-rich tuff and lapillistone (bT/bL) See Figure 6.	Clast-supported, well sorted (σ_Φ= 1.5–2), dense to poorly vesicular angular juvenile scoria clasts 0.5–50 mm in diameter; vesicles occur in low abundances (10–20 vol. %) are spherical to elongate in shape or coalesced and 0.02–3 mm in diameter; free olivine crystals and micro-xenoliths present in variable abundances (<15 vol. %); basement lithic clasts are rare.	Beds 3–>100 cm thick; defined by grainsize; commonly occurs interstratified with bspelT/bspelL.
Massive to bedded juvenile clast-rich lapillistone (mbL)	Compositionally similar to bsL (above); clast-supported moderately to well sorted (estimated) scoria lapilli and coarse ash; rare lithic clasts <6 cm in diameter.	Massive to very crudely bedded on a metre-scale defined by grainsize.

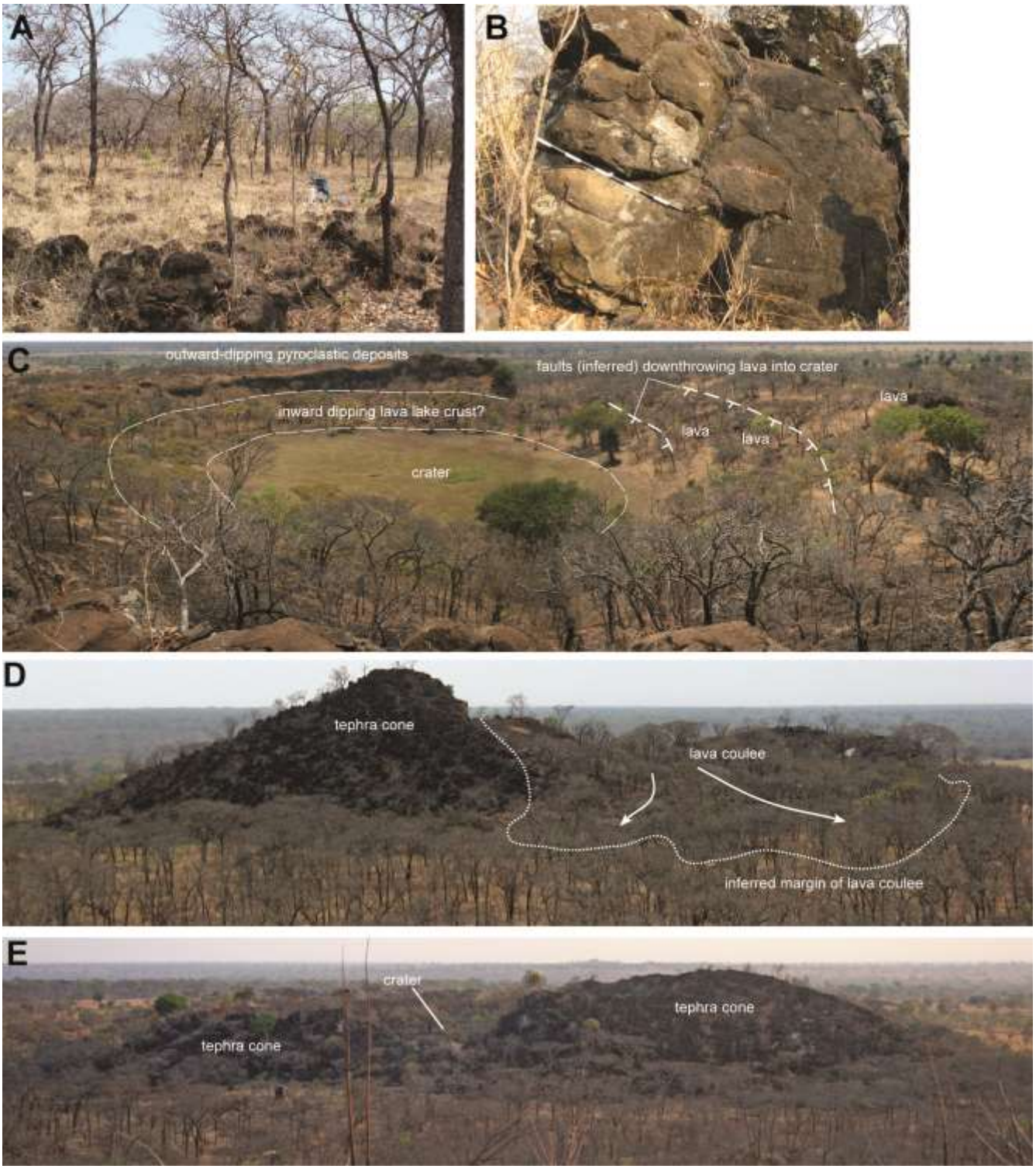
Table 3. Pyroclastic lithofacies of the Igwisi Hills volcanoes.



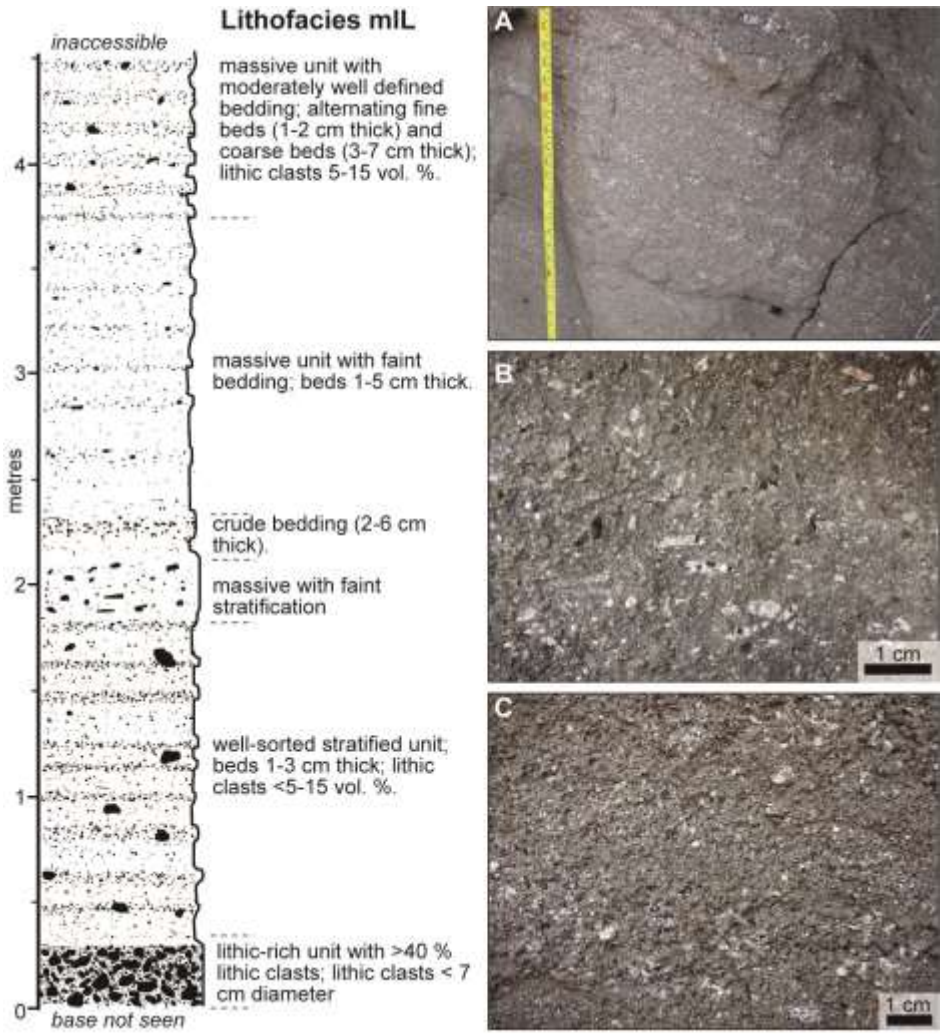
1189
1190


solid effusive rocks
dense, lithic-bearing lava
olivine-bearing dense to poorly vesicular lava
pyroclastic rocks
bedded and stratified scoria-rich and pelletal clast-rich tuffs and lapillistones (bpeltT/bpelL and bT/bL)
masive to bedded juvenile clast-rich lapillistone (mbL)
massive to stratified lithic-bearing tuffs/lapillistones (mlT/mlL)
drift
lacustrine mud and silt
talus
soil
fault (inferred)
contours in 2 m intervals
IH15* cosmogenic sample site
0
metres
500
N
TRENCH 1
TRENCH 2
TRENCH 3
TRENCH 4
IH61
IH52
IH15
NE volcano
central volcano
SW volcano
inferred extent of lava flow
lava fed from perched lava lake
extent of lava unknown
n=55
SW
Ce
NE
bedding dip (degree)
1120 m
1110 m
1106 m
1104 m
1146 m
1124 m
1144 m
1130 m
100 m
no vertical exaggeration

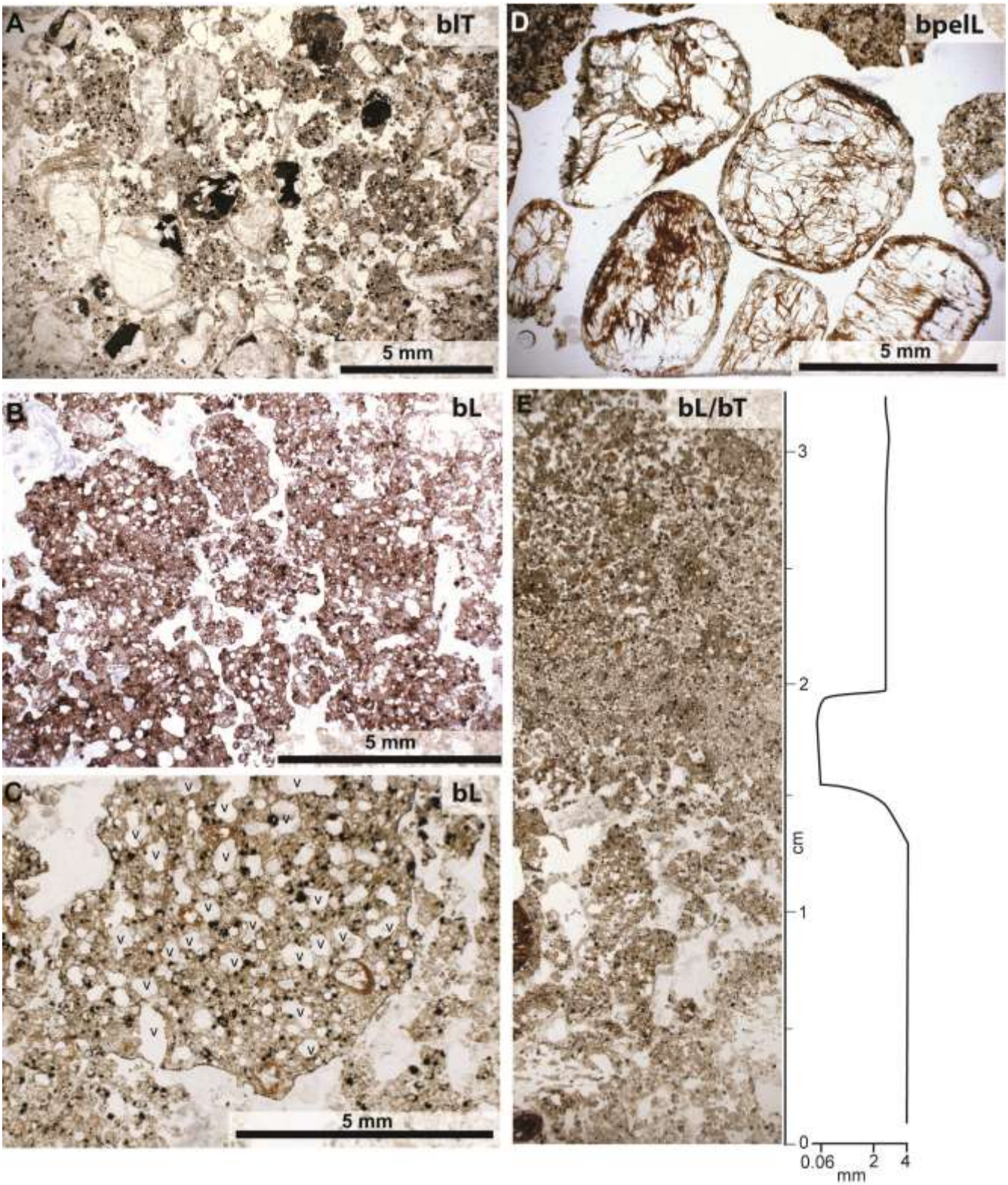
1192



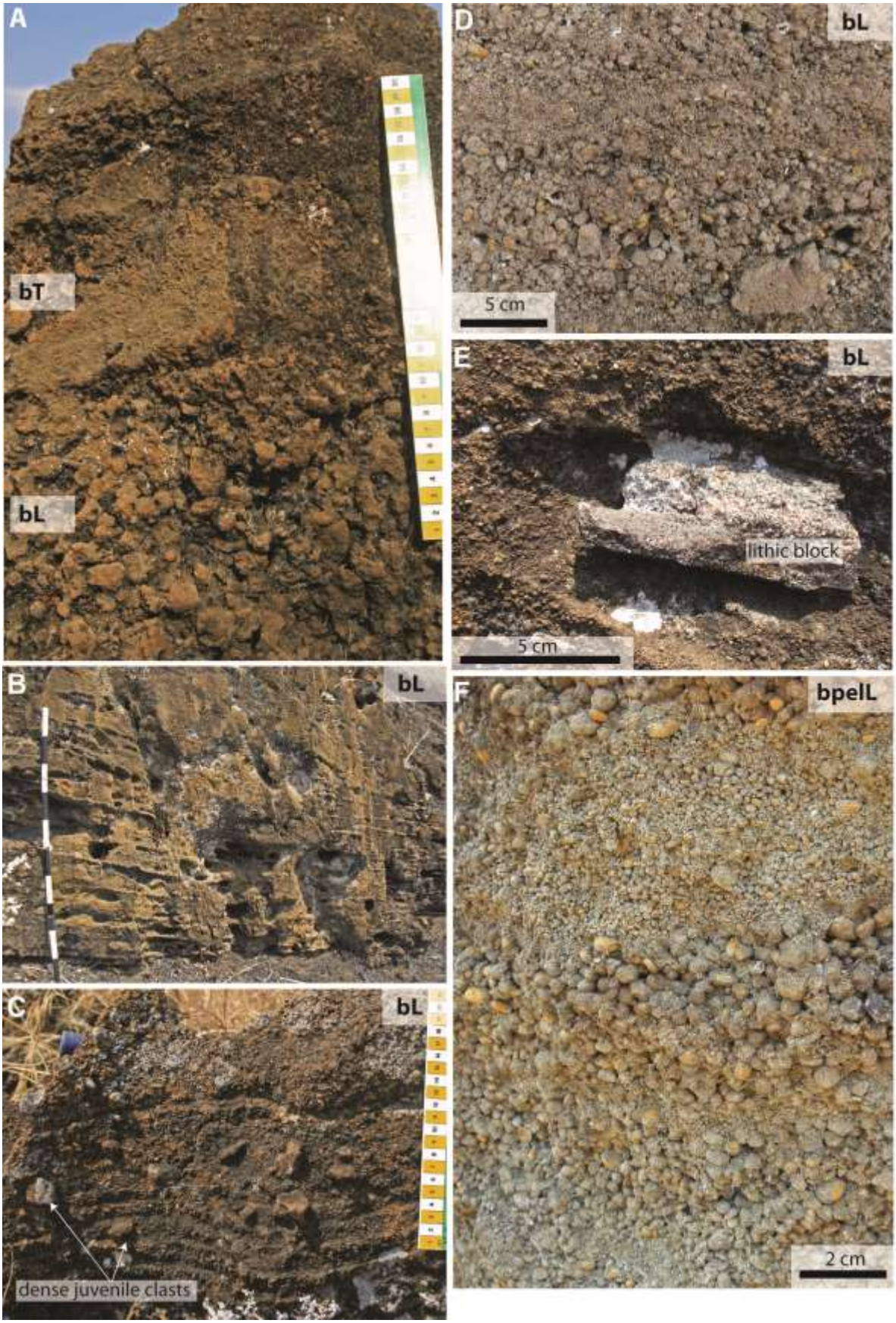
1193
1194
1195
1196
1197


Lithofacies mIL
inaccessible
massive unit with moderately well defined bedding; alternating fine beds (1-2 cm thick) and coarse beds (3-7 cm thick); lithic clasts 5-15 vol. %.
massive unit with faint bedding; beds 1-5 cm thick.
crude bedding (2-6 cm thick).
massive with faint stratification
well-sorted stratified unit; beds 1-3 cm thick; lithic clasts <5-15 vol. %.
lithic-rich unit with >40 % lithic clasts; lithic clasts < 7 cm diameter
base not seen
metres
0
1
2
3
4
A
B
1 cm
C
1 cm

1198
1199

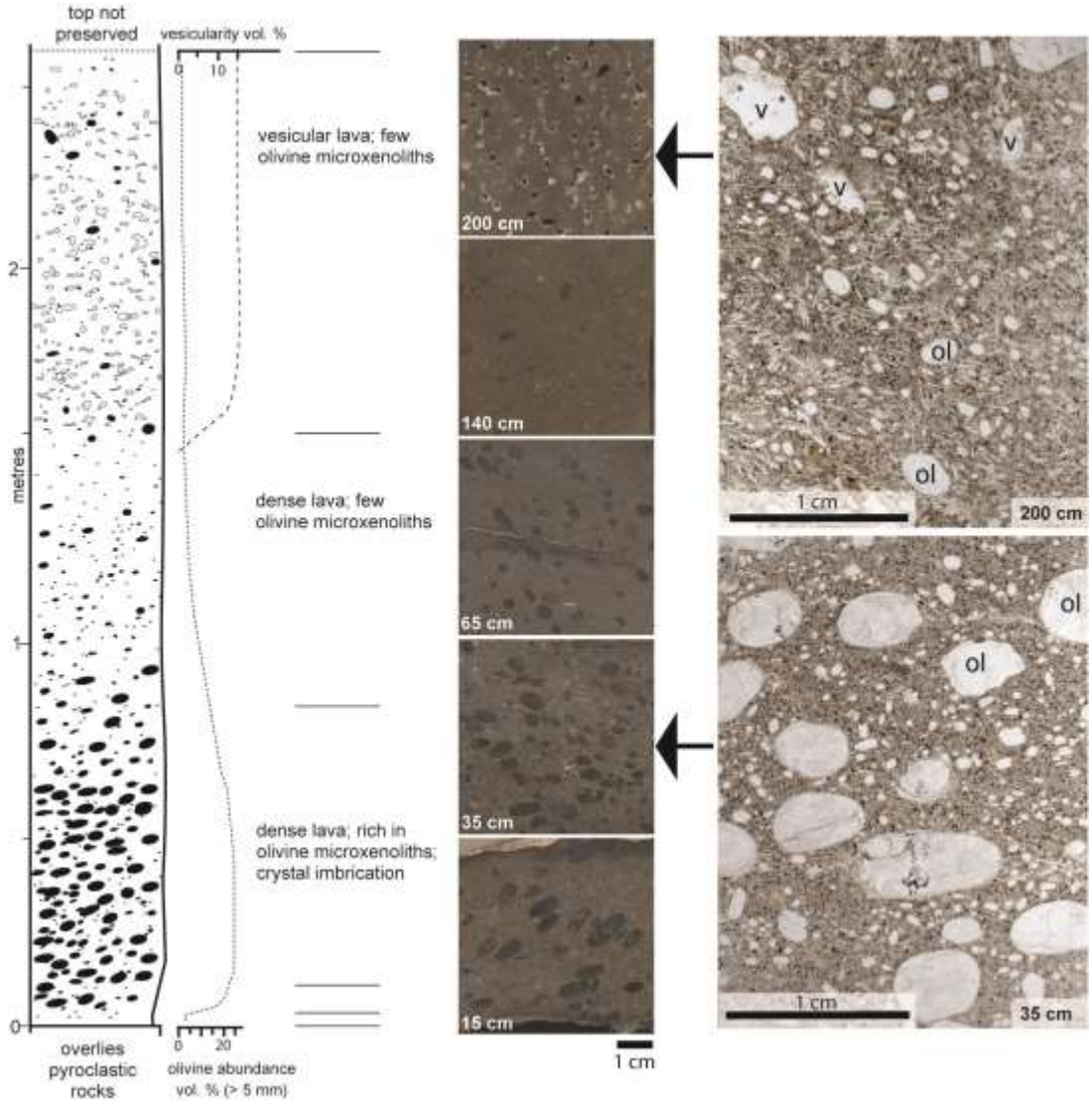


1200
1201
1202
1203

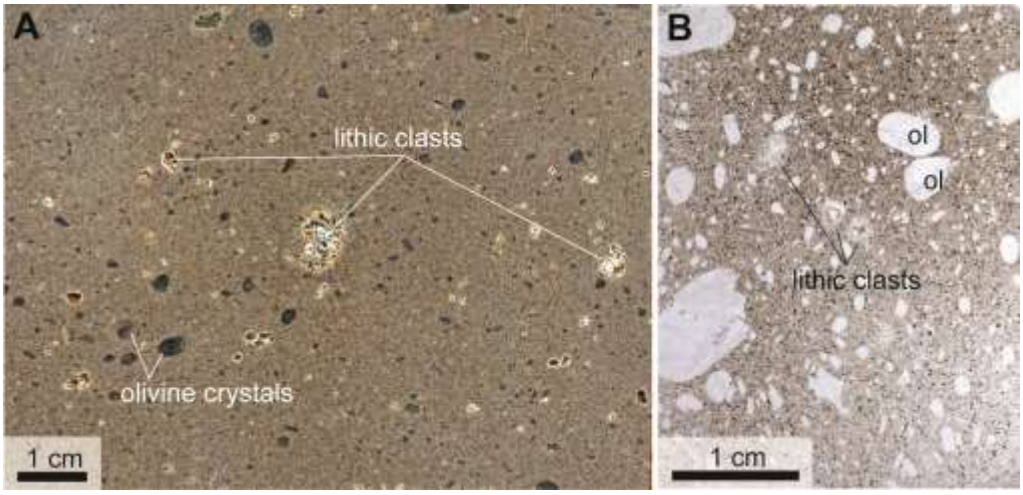

A
bT
bL
B
bL
C
bL
dense juvenile clasts
D
bL
5 cm
E
bL
lithic block
5 cm
F
bpelL
2 cm

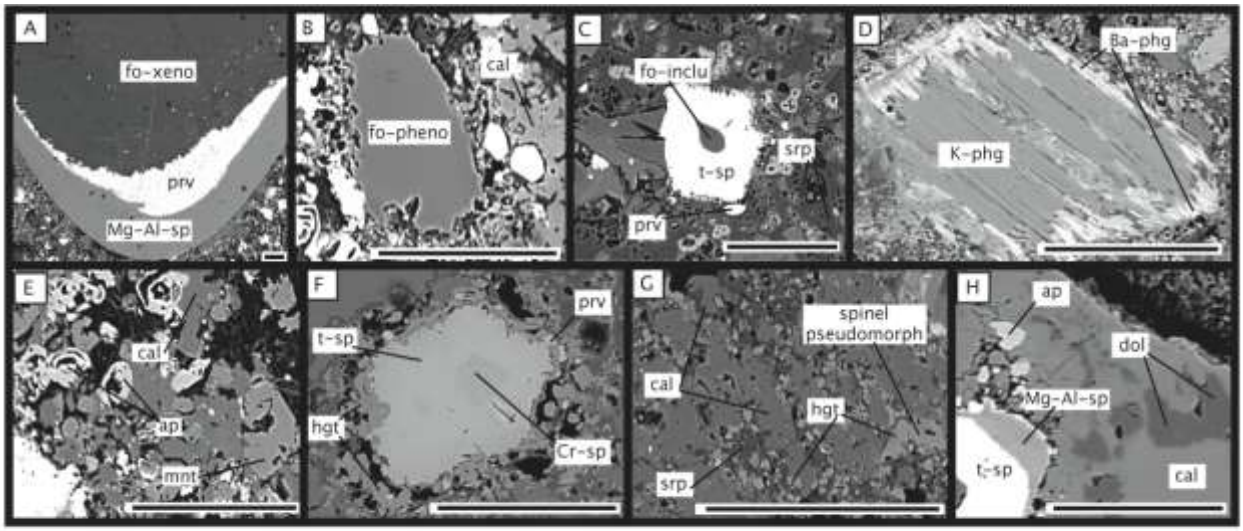
1204
1205

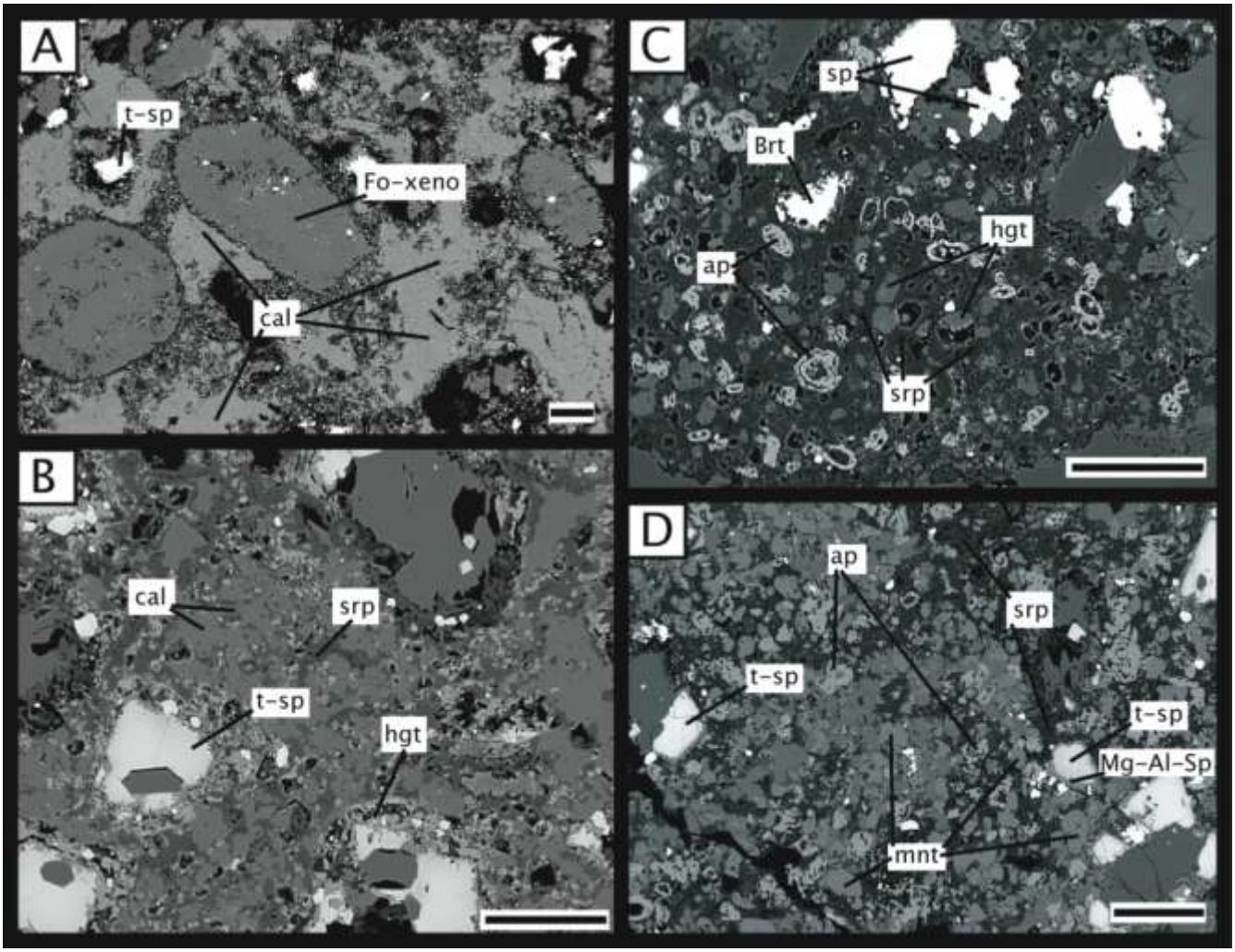
1206

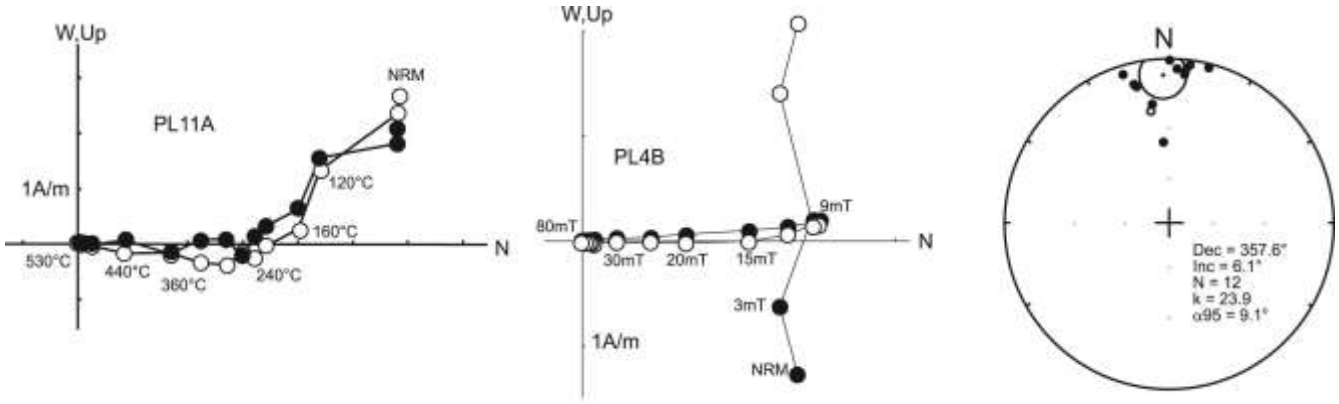


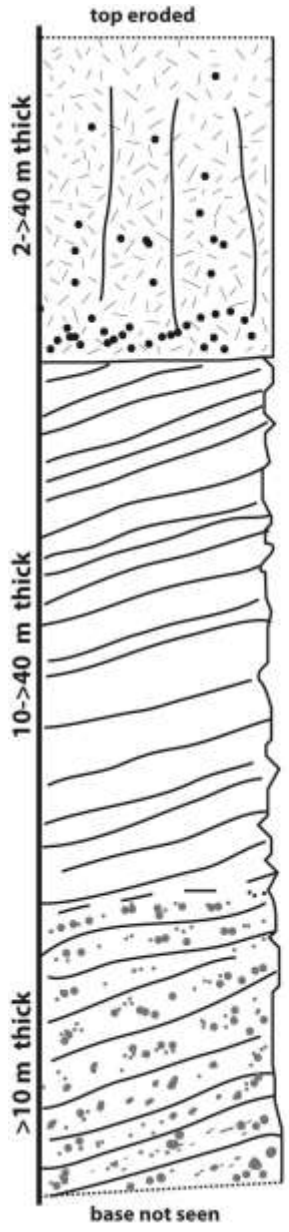
1207
1208
1209
1210
1211
1212
1213
1214


A
lithic clasts
olivine crystals
1 cm
B
ol
ol
lithic clasts
1 cm


A
fo-xeno
prv
Mg-Al-sp
B
cal
fo-pheno
C
fo-inclu
srp
t-sp
prv
D
Ba-phg
K-phg
E
cal
ap
mnt
F
prv
t-sp
hgt
Cr-sp
G
spinel
pseudomorph
cal
hgt
srp
H
ap
dol
Mg-Al-sp
t-sp
cal


A
t-sp
Fo-xeno
cal
B
cal
srp
t-sp
hgt
C
sp
Brt
hgt
ap
srp
D
ap
srp
t-sp
t-sp
Mg-Al-Sp
mnt

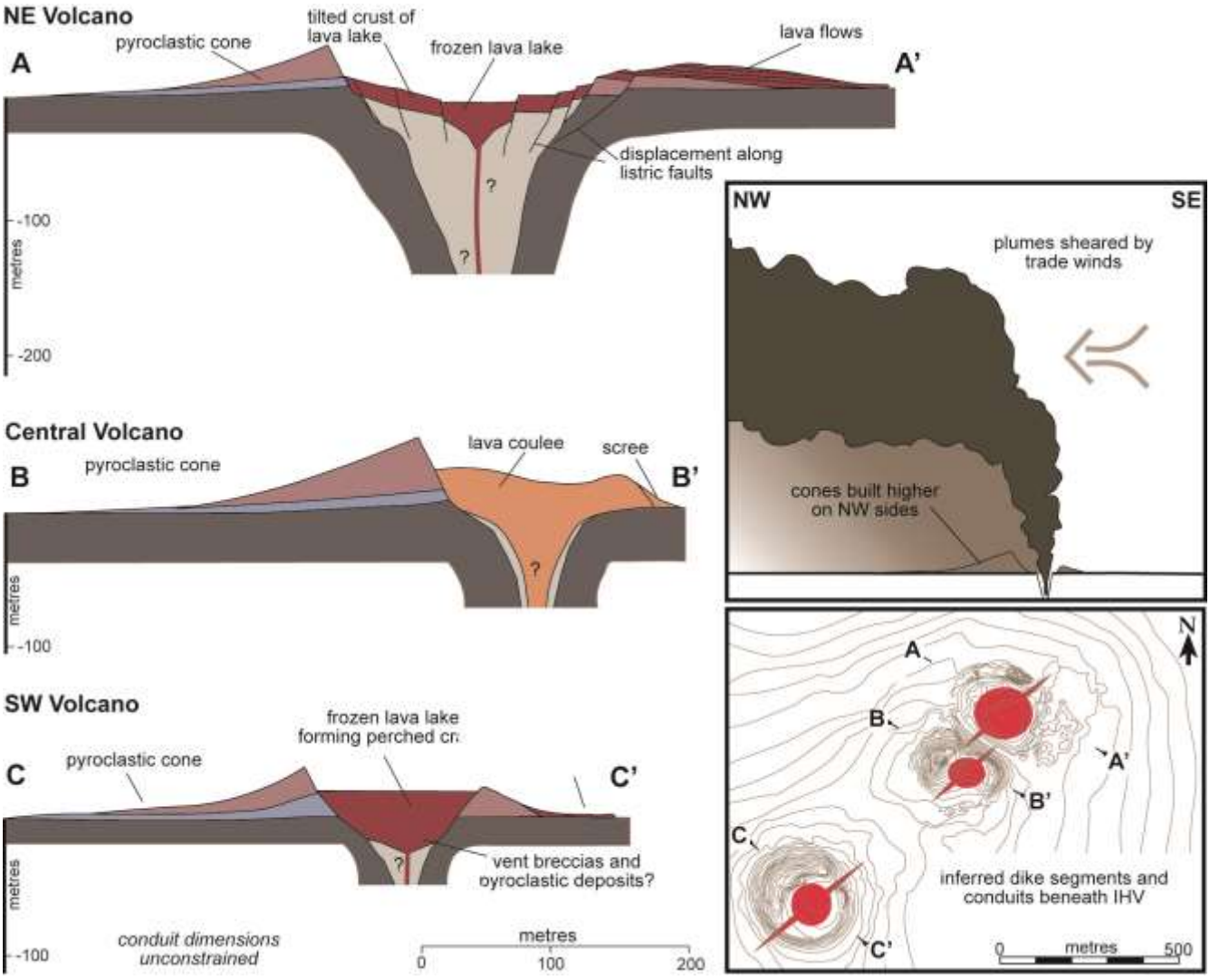

W,Up
PL11A
NRM
1A/m
120°C
160°C
530°C
440°C
360°C
240°C
N
W,Up
PL4B
80mT
30mT
20mT
15mT
9mT
3mT
NRM
1A/m
N
Dec = 357.6°
Inc = 6.1°
N = 12
k = 23.9
α95 = 9.1°



Phase 3
Lava flows
Late-stage effusion of degassed and partially crystallised magma that fed lava flows and a lava coulee; lavas form plugs, lava lakes and extra-crater lava flows.

Phase 2
Juvenile-rich tuffs and lapillistones
Fallout from weak, unsteady eruption plumes sheared by trade winds; construction of pyroclastic edifices composed of poorly vesicular juvenile pyroclasts and pelletal lapilli; pyroclastic edifices, are constructed higher on NW side of volcanoes.

Phase 1
Lithic-bearing tuffs and lapillistones
Fall deposits generated during explosive eruptions that excavated country rock and generated unsteady eruption columns.


NE Volcano
A
A'
pyroclastic cone
tilted crust of lava lake
frozen lava lake
lava flows
displacement along listric faults
?
?
-100
metres
-200
Central Volcano
B
B'
pyroclastic cone
lava coulee
scree
?
metres
-100
SW Volcano
C
C'
pyroclastic cone
frozen lava lake forming perched cr
vent breccias and pyroclastic deposits?
?
metres
-100
conduit dimensions unconstrained
metres
0
100
200
NW
SE
plumes sheared by trade winds
cones built higher on NW sides
N
A
B
A'
B'
C
C'
inferred dike segments and conduits beneath IHV
0
metres
500